

Isovector spin-singlet ($T=1, S=0$) and isoscalar spin-triplet ($T=0, S=1$) pairing interactions and spin-isospin response

H. Sagawa*

RIKEN, Nishina Center, Wako, 351-0198, Japan

and

Center for Mathematics and Physics, University of Aizu,

Aizu-Wakamatsu, Fukushima 965-8560, Japan

C. L. Bai†

School of Physical Science and Technology, Sichuan University, Chengdu 610065, China

G. Colò‡

Dipartimento di Fisica, Università degli Studi di Milano

and

INFN, Sezione di Milano, 20133 Milano, Italy

PACS REF: 21.60.Jz, 21.65.Ef, 24.30.Cz, 24.30.Gd

Abstract

We review several experimental and theoretical advances that emphasise common aspects of the study of spin-singlet, $T = 1$, and spin-triplet, $T = 0$, pairing correlations in nuclei. We first discuss several empirical evidences of the special role played by the $T = 1$ pairing interaction. In particular, we show the peculiar features of the nuclear pairing interaction in the low density regime, and possible outcomes such as the BCS-BEC crossover in nuclear matter and, in an analogous way, in loosely bound nuclei. We then move to the competition between $T = 1$ and $T = 0$ pairing correlations. The effect of such competition on the low-lying spectra is studied in $N = Z$ odd-odd nuclei by using a three-body model; in this case, it is shown that the inversion of the $J^\pi = 0^+$ and $J^\pi = 1^+$ states near the ground state, and the strong magnetic dipole transitions between them, can be considered as a clear manifestation of strong $T = 0$ pairing correlations in these nuclei. The effect of $T = 0$ pairing correlations is also quite evident if one studies charge-changing transitions. The Gamow-Teller (GT) states in $N = Z + 2$ nuclei are studied here by using self-consistent Hartree-Fock Bogoliubov (HFB) plus Quasi-particle Random Phase Approximation (QRPA) calculations in which the $T = 0$ pairing interaction is taken into account. Strong GT states are found, near the ground state of daughter nuclei; these are compared with available experimental data from charge-exchange reactions, and such comparison can pinpoint the value of the strength of the $T = 0$ interaction. Pair transfer reactions are eventually discussed: while two-neutron transfer has been long proposed as a tool to measure the $T = 1$ superfluidity in the nuclear ground states, the study of deuteron transfer is still in its infancy, despite its potential interest in revealing effects coming from both $T = 1$ and $T = 0$ interactions. We also point out that the reaction mechanism may mask the strong pair transfer amplitudes predicted by the HFB calculations, because of the complexity arising from simultaneous and sequential pair transfer processes.

1. Introduction — superfluidity in nuclei

The effective nucleon-nucleon interactions that are employed within self-consistent mean-field approaches have recently reached a high level of sophistication, and have become quite successful in describing many nuclear properties. Though they can be based on different kinds of ansatz, central, spin-orbit, and tensor terms show up all ways. In open-shell nuclei the pairing interaction or, in fact, its isovector ($T = 1, S = 0$) part, has been originally introduced to account for the odd-even binding energy staggering, the gap in the excitation spectrum of even-even and odd- A nuclei [1, 2, 3], the moment of inertia of deformed nuclei [2] and also the fission barrier of actinide nuclei (cf. p. 158 of [3]). In the literature, only the spin-singlet $T = 1$ pairing has been mainly discussed in nuclear physics, since the large spin-orbit splitting prevents to couple a spin-triplet ($T = 0, S = 1$) pair in the ground state [4, 5]. Another reason for this is that the neutron excess along the stability line of the nuclear chart suppresses the proton-neutron pairing for medium-mass and heavy nuclei. The recent availability of radioactive beams has opened up new opportunities to measure structure properties of unstable nuclei along the $N = Z$ line, strongly enhancing the possibility to measure new properties of nuclei such as pairing correlations related with the spin-triplet $T = 0$ pairing [6]. It is thus quite interesting and important to study the competition between the spin-singlet $T = 1$ and the spin-triplet $T = 0$ pairing interactions in $N \approx Z$ nuclei, and seek an experimental evidence for their competition in the energy spectra and the transition rates.

One of the widely used mean-field approaches is based on zero-range Skyrme forces: Hartree-Fock (HF) plus Bardeen-Cooper-Schrieffer (BCS) equations [7, 8] or Hartree-Fock-Bogoliubov (HFB) equations [8, 9], which include the pairing interaction, can be, and have been solved, to study the ground state properties of the open-shell nuclei [10, 11, 12, 13]. On top of this ground-state so-

*e-mail: sagawa@ribf.riken.jp

†e-mail: bclphy@scu.edu.cn

‡e-mail: colo@mi.infn.it

lutions, the self-consistent Quasi-particle Random-Phase-Approximation (QRPA) has been adopted by many authors to study the collective excited states [8, 14, 15, 16, 17, 18, 19].

The parameters that characterize the effective interactions like the Skyrme ones can be fitted by using empirical properties of uniform nuclear matter, as well as few ground-state (or sometimes excited state) properties of finite nuclei. However, some channels of the interactions are not well constrained, one of the clearest examples being the pairing interaction between protons and neutrons in the isoscalar spin-triplet ($T = 0$, $S = 1$) channel. Indeed, there is no consensus on the observables that can be directly related to such channel, and not yet unambiguous signatures of strong neutron-proton particle-particle correlations, despite several efforts [20, 21, 22, 23, 24, 25, 26].

It has been well known that one of the effects of the bare isoscalar spin-triplet force is to give rise to the deuteron bound state. Although some speculations have been made about the relevance of a n-p pairing force in nuclei with $N = Z$, there is not unambiguous evidence of its effects, let alone evidence of a p-n condensate. In Ref. [25], it has been shown that ordinary bound nuclei are dominated by spin-orbit effects but on the other hand, if such effects can be made less important and one considers either very large nuclei or nuclei with low angular momentum orbitals close to the Fermi surface, then n-p pairing does manifest itself strongly.

Low-lying states of nuclei having a neutron and a proton outside a relatively closed core may be good candidates to study n-p pairing, as far as the two particles lie in the same orbital. However, collective states are probably better candidates to extract more firm and general information. In this respect, effects of isoscalar pairing may be present in charge-exchange excitations and related phenomena. Indeed, in self-consistent Skyrme QRPA calculations it can be shown that the Gamow-Teller Resonance (GTR) is only sensitive to $T = 0$ pairing, while the Isobaric Analog Resonance (IAR) is only sensitive to $T = 1$ pairing [27]. This is related to the zero-range character of Skyrme forces, but it remains to a large extent true when finite-range pairing interactions are adopted [16] — also in the context of Relativistic Mean Field (RMF) calculations [19]. In particular, in Refs. [16, 28, 29] it has been shown that in self-consistent HFB plus QRPA calculations the isoscalar pairing interaction shifts some low-energy Gamow-Teller (GT) strength downwards, so that by fitting the n-p pairing strength (at least locally) one can account for the β -decay half-lives in neutron-rich nuclei. The isoscalar pairing interaction is also important for the double- β decay [30]. However, not only the isoscalar pairing but also other terms of the effective interaction affect in an important way the main peak and low-energy part of the GT strength [31, 32, 33, 34, 35]: in particular, this is true for the spin-orbit one-body potential, the spin two-body terms and also tensor terms. One goal of Ref. [27] was to point out the necessity of improving Skyrme forces, and this goal has been reached in Ref. [36].

In short, although it has been put into evidence clearly that both the GTR and the higher order multipole of charge-exchange transitions, such as the spin-dipole and spin-quadrupole transitions, will receive contribution from

both the isoscalar and the isovector pairing forces, firm constraints for the isoscalar pairing have not been extracted until very recently. One of the reasons is that in many of the previous studies the nuclei that have been considered possess neutron excess and are not close to the regions where isoscalar pairing effects are expected to show up. Thus, an important purpose of this contribution is to demonstrate that one is bound to consider specific nuclei and/or specific properties to pin down unambiguous information about isoscalar pairing.

2. Nuclear structure and isovector spin-singlet pairing interaction

2.1. Odd-even mass staggering

The nuclear binding energies are found to show a systematic variation depending on the even or odd values of Z and N ,

$$\Delta\mathcal{B} = \begin{cases} \Delta & \text{for } Z = \text{even and } N = \text{even}, \\ 0 & \text{for } A = \text{odd}, \\ -\Delta & \text{for } Z = \text{odd and } N = \text{odd}, \end{cases} \quad (1)$$

where $A = N + Z$. To illustrate this point, the separation energy which is the difference of binding energies $\mathcal{B}(A)$ of two neighboring nuclei,

$$S_n(A) = \mathcal{B}(A) - \mathcal{B}(A - 1), \quad (2)$$

is shown in Fig. 1 in the case of Sn isotopes. The staggering of $S_n(A)$ is certainly due to the extra binding of even- N Sn isotopes. Specific filters can be introduced to prove this evidence. In particular, the 3-point formula for the neutron pairing gap, or pairing index, reads

$$\begin{aligned} \Delta^{(3)}(N) &= (-)^{A+1} \frac{\mathcal{B}(N+1) - 2\mathcal{B}(N) + \mathcal{B}(N-1)}{2} \\ &= (-)^{A+1} \frac{S_n(A+1) - S_n(A)}{2}. \end{aligned} \quad (3)$$

This pairing index is expected to be proportional to the extra binding energy Δ in Eq. (2). This is of course to be considered as a reasonable first approximation. Subtle interferences between pairing effects and mean-field effects are discussed in Refs. [37, 38, 12]. The 3-point formula centered in the odd- A nucleus can remove the major shell effect on the pairing index [37], while the 4- and 5-point formulas were also considered to avoid a large shell effect in the systematic studies of Refs. [38, 12]. Again, to a first approximation, the pairing index can be parametrized as

$$\Delta^{(3)}(A) \approx 12/A^{1/2} \text{ MeV}, \quad (4)$$

in the broad region of the mass table $16 < A < 250$ [1].

As mentioned in the Introduction, HF-BCS or HFB are the standard theories to describe pairing in nuclei. In such frameworks, the quasi-particle energies are expressed as

$$E_k = \sqrt{(\varepsilon_k - \lambda)^2 + \Delta_k^2}, \quad (5)$$

where ε_k and Δ_k are the single-particle energies and (state-dependent) pairing gaps, respectively, and λ is the chemical potential. If we assume that the ground state of the odd nucleus is a quasi-particle state on top of the

even core, then the comparison between Eqs. (3) and (5) clearly shows that $E_k \approx \Delta_k \approx \Delta^{(3)}$.

Only for n-n and p-p pairing such clear filters exist and point to values of the pairing gap that are consistent with other observables like those mentioned at the start of the Introduction. From a theoretical viewpoint, however, the omission of n-p pairing has been found to be not fully justified already fifty years ago (see [20] and references therein). The complete generalized isospin pairing theory can be introduced [20, 21]. In the BCS version, the Cooper pairs are not simply formed by two identical nucleons in time-reversed states, $|k\rangle$ and $|\tilde{k}\rangle$, but rather one can assume pairs made up in a general way with the four states $|k, \pi\rangle$, $|k, \nu\rangle$, $|\tilde{k}, \pi\rangle$ and $|\tilde{k}, \nu\rangle$. In such generalized theory, nonetheless, the quasi-particle energy keeps the same form as in (5), and the pairing gap reads

$$\Delta_k^2 = |\Delta_{k\pi, k\nu}|^2 + |\Delta_{k\pi, \tilde{k}\pi}|^2 + |\Delta_{k\pi, \tilde{k}\nu}|^2. \quad (6)$$

In HFB one can even further generalize the wave function, by considering pairs that do not correspond to time-reversed states.

There is a subtle interplay between pairing and deformation: the first calculations [39] showed that different types of pairing arise if the nucleus is spherical, axially symmetric or triaxial, respectively. Only light nuclei with $N \approx Z$ are candidates for n-p pairing. Neutron excess and/or large spin-orbit splittings hinder n-p pairing as discussed in the Introduction.

One may wonder whether the results for the dominance of the different kinds of pairing are confirmed within calculations that employ realistic effective interactions. In the work of Ref. [25], extensive HFB calculations have been performed with the hope of clarifying if and where $T = 0$ pairing can dominate over $T = 1$ pairing. A simple yet realistic choice has been adopted for the mean-field Hamiltonian, that is, a Woods-Saxon potential plus spin-orbit. The pairing forces have been chosen to be zero-range form, namely

$$V^{T=1}(\vec{r}_1, \vec{r}_2) = \hat{P}_s V_0 \delta(\vec{r}_1 - \vec{r}_2), \quad (7)$$

and

$$V^{T=0}(\vec{r}_1, \vec{r}_2) = \hat{P}_t f V_0 \delta(\vec{r}_1 - \vec{r}_2), \quad (8)$$

where \hat{P}_s and \hat{P}_t are the projectors onto the spin-singlet and spin-triplet channels, respectively:

$$\hat{P}_s = \frac{1}{4} - \frac{1}{4} \sigma_p \cdot \sigma_n, \quad \hat{P}_t = \frac{3}{4} + \frac{1}{4} \sigma_p \cdot \sigma_n. \quad (9)$$

If these forces are adjusted so to reproduce at best the matrix elements of realistic shell-model calculations, the ratio f between the $T = 0$ and $T = 1$ pairing strengths turns out to be $f \approx 1.6$ -1.7. It has been found that, with the exception of few light nuclei, $T = 0$ pairing cannot dominate the ground-state of stable nuclei despite its larger strength. The reason is precisely the magnitude of the spin-orbit splittings. In fact, if the nuclei are large enough so that the spin-orbit effects are weakened, $T = 0$ pairing can take over; such nuclei have mass larger than $A \approx 130 - 140$ and are mostly prone to be unbound via proton emission.

2.2. Low-energy collective excitations

In Fig. 2 we display the low part of the excitation spectra in few Sn isotopes. As is well known, and discussed

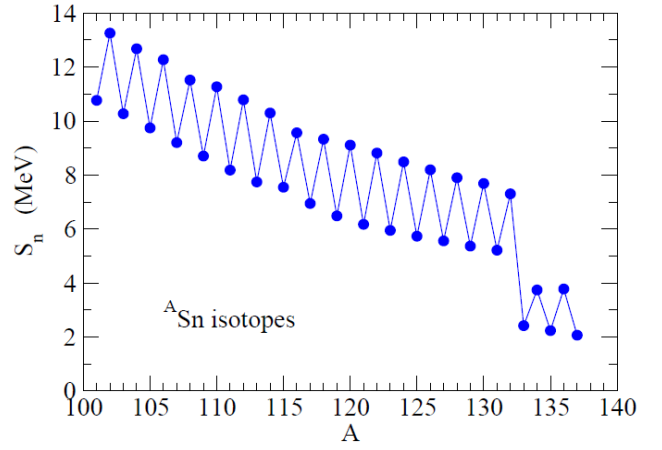


Fig. 1: Separation energy of Sn isotopes, as defined in the text in Eq. (2).

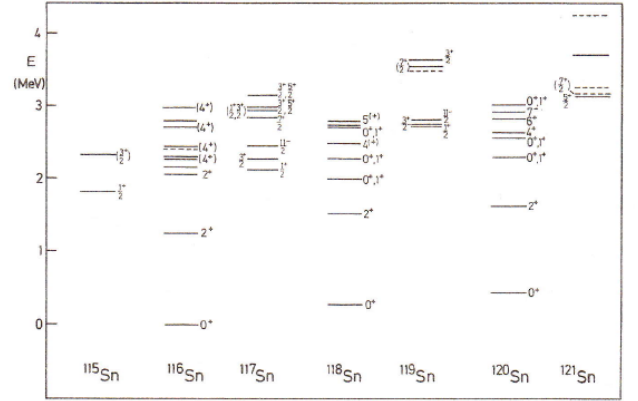


Fig. 2: Low-lying part of the energy spectra of few Sn isotopes. The figure is taken from Ref. [8]. See the discussion in the main text.

above, in odd- N isotopes the unpaired neutron does not feel pairing correlations and can occupy several orbitals close to one another, so that there is no gap in the excitation spectra. In even- N isotopes, the lowest state is a 2^+ state. If we interpret this state as a two quasi-particle (2qp) excited state, its excitation energy with respect to the ground-state 0qp should be written as

$$E_{2qp} - E_{0qp} = 2E_{qp} \approx 2\Delta, \quad (10)$$

where the last approximation stems from the idea that both excited quasi-particles lie at the Fermi surface. This latter equation has also a very transparent interpretation, namely it shows that the minimal energy to create an excited state of 2qp type corresponds to breaking two Cooper pairs in order to recouple the particles to different angular momenta.

In the tin region, the value of Δ is expected to be about 1.0 MeV [cf. Eq. (4)]. However, the excitation energies of the 2^+ states, as visible in Fig. 2, are observed to be smaller than 2 MeV because of extra correlation energy. In fact, in QRPA, that is, the standard theory for such vibrational states, the energy of a collective state $\hbar\omega$ can

be schematically written as

$$\hbar\omega = \sqrt{(E_{2qp} - E_{0qp})^2 + \langle V \rangle^2}, \quad (11)$$

where $\langle V \rangle$ is an average value of the residual interaction between quasi-particle states (cf. Ref. [8] for a complete account of QRPA with detailed formulas). In a magic nucleus, in which pairing does not manifest itself, the residual interaction would be only of p-h type, and the p-h channel of the nuclear effective Hamiltonian is in a sense uniquely sensitive to a given multipole component (e.g., quadrupole if low-lying 2^+ states are under study). In open-shell nuclei like the Sn isotopes, the p-p force plays an important role, and low-lying states are sensitive both to its $J = 0$ component which is usually called pairing force and to its multipole component. Last but not least, one should remind that not only energies carry signatures of the p-p force as well as of other components of the nuclear Hamiltonian, but electromagnetic transition probabilities $B(EL)$ do it as well [40]. Approximately, one could say that they are inversely proportional to energies.

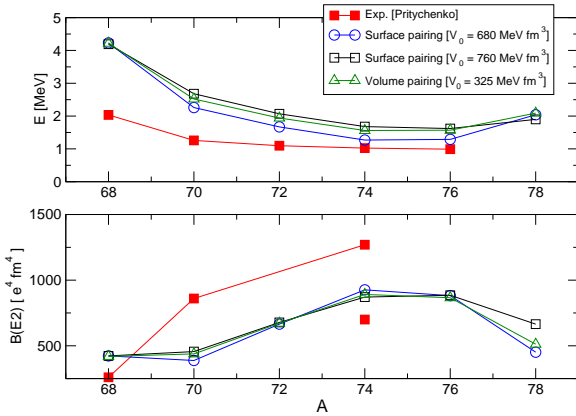


Fig. 3: Energies and electromagnetic transition probabilities of the low-lying Ni isotopes calculated with different pairing forces and compared with the experimental data.

To disentangle such effects is not an easy task. Along the last decade, fully microscopic QRPA calculations have become available and have been extensively used to study low-lying vibrational excitations. In Ref. [41], for instance, the global performance of QRPA with Skyrme forces has been tested by calculating basically all nuclei that are experimentally known. Unfortunately, only global conclusions have been extracted, and the specific role of the pairing force has not been pinned down as only one type of force has been used, namely the so-called volume pairing force already defined in Eq. (7). This is the closest possible to a pairing force with constant matrix elements G , since it is easy to understand that if all wave functions have similar integral values within the nuclear volume the radial matrix elements of such force cannot vary much. Starting from the work [42], it has been suggested that the pairing force should better be density dependent, and

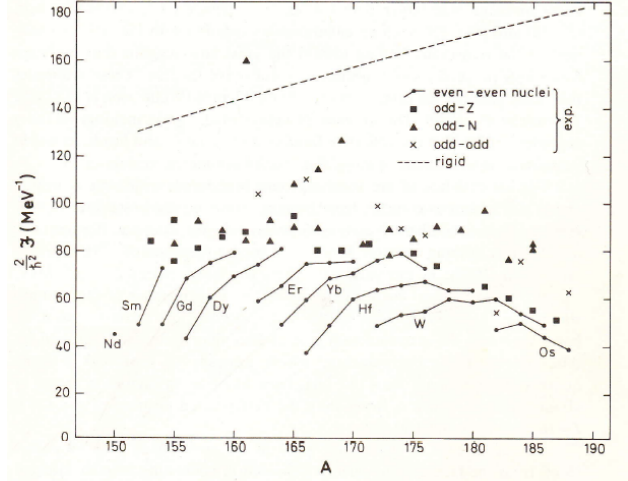


Fig. 4: Values of the moment of inertia of deformed nuclei with mass $150 < A < 188$. The figure is taken from Ref. [2].

may be taken as

$$V_{surface}^{T=1}(\vec{r}_1, \vec{r}_2) = \hat{P}_s V_0 \left(1 - x \left(\frac{\rho}{\rho_0} \right)^\gamma \right) \delta(\vec{r}_1 - \vec{r}_2), \quad (12)$$

with $x = 1$ and γ often taken as 1 for simplicity but in principle arbitrary. Such an interaction is called surface pairing force, because if ρ_0 is around the saturation density the parameters can be chosen so to enhance pairing at the surface. Several studies have been shown that the low-lying states, and in particular their transition probabilities, are very sensitive to the choice of the pairing force (see, e.g., Ref. [44]). Although some authors have expressed preference for a surface pairing force in this context [43], no conclusive study exists. We show in Fig. 3 some results for the energy and reduced transition probability of the low-lying 2^+ states along the neutron-rich part of the Ni isotope chain. The surface and volume pairing forces have been chosen so that the values of the pairing gaps do not differ by more than 20%. Only in ^{78}Ni the solution can be either superfluid or normal according to the strength of the pairing force. This affects mainly the quadrupole transition probability.

It would be of paramount importance to improve our understanding of the effects of different type of pairing forces in the low-lying nuclear spectroscopy. 3^- or higher multipole states can be of course discussed on equal footing. This could pave the way to a better understanding of how pairing evolves far from the stability valley, because the properties of low-lying vibrational states of even-even nuclei are among the very first observables that one can collect when producing new, exotic nuclei. At the same time, we stress that we are so far concerned only with the $T = 1$ pairing force. The microscopic origin of the density dependence of the pairing force, and/or the contribution to it coming from polarization effects, is outside the scope of the present paper.

2.3. Moments of inertia of deformed nuclei

The energy spectrum of a deformed nucleus is characterized by the presence of rotational bands in which levels

with angular momentum I have energies that scale like

$$E_I = E_0 + \frac{I(I+1)}{2\mathfrak{I}}, \quad (13)$$

where E_0 is the energy of the so-called bandhead, that is, the level with a given intrinsic configuration and zero-point rotational motion while \mathfrak{I} is the moment of inertia of the nucleus. From the experimental point of view, the measurement of the γ -transitions between the states (13) provides the value of the energy of these states and consequently of the moment of inertia. From the theoretical point of view, it is possible to perform so-called cranking calculations, in which the nuclear Hamiltonian is solved with a constraint ωj_x that corresponds to a rotation around the x -axis (we assume here that the nucleus has the z -axis as a symmetry axis and need to rotate around a perpendicular axis). In particular, one can obtain the value of the moment of inertia within the framework of second order perturbation theory (where the cranking term ωj_x plays the role of the perturbing field). The moment of inertia obtained in this way, so called Inglis's one, is given by

$$\mathfrak{I}_{\text{Inglis}} = 2 \sum_{p,h} \frac{|\langle p | j_x | h \rangle|^2}{\varepsilon_p - \varepsilon_h}, \quad (14)$$

where the labels p and h corresponds to particle and hole states, since the perturbing field creates p - h pairs at lowest order. It is known that the Inglis moment of inertia is equivalent to the moment of inertia of a rigid body. Formally, this is proven within the harmonic oscillator potential approximation (cf. p. 77 of Ref. [45]); however, the result can be empirically checked to be the same in more realistic cases.

In the presence of superfluidity, the ground state is represented by the BCS vacuum and the lowest order p - h excitations are replaced by the two quasi-particle ones. Accordingly, the moment of inertia can be obtained as

$$\mathfrak{I}_{\text{BCS}} = 2 \sum_{\alpha,\beta} \frac{|\langle \alpha | j_x | \beta \rangle|^2 (u_\alpha v_\beta - u_\beta v_\alpha)^2}{E_\alpha + E_\beta}, \quad (15)$$

where E labels the quasi-particle energy [Eq. (5)], and u, v are the BCS unoccupation and occupation factors with $u_k^2 + v_k^2 = 1$. The formula (15) gives in general smaller values than Eq. (14) since the denominator $E_\alpha + E_\beta$ is larger than $\varepsilon_i - \varepsilon_j$, and $(u_\alpha v_\beta - u_\beta v_\alpha)^2$ is smaller than one. The experimental values for the moment of inertia are compared with the calculated ones in Fig. 4. The quenching with respect to the rigid-body value is one of the evidences of superfluidity in nuclei.

2.4. Pairing correlations at low density and BCS-BEC crossover

The pairing correlations at low nucleon density are of special interest, since the theoretical predictions for low-density uniform matter suggest that the pairing gap may take, at around 1/10 of the normal nuclear density, a value which is considerably larger than that around the normal density, both in the case of the isovector spin-singlet and the isoscalar spin-triplet channel (see e.g. [24] and references therein). This feature is expected to have direct relevance for the properties of neutron stars, especially those

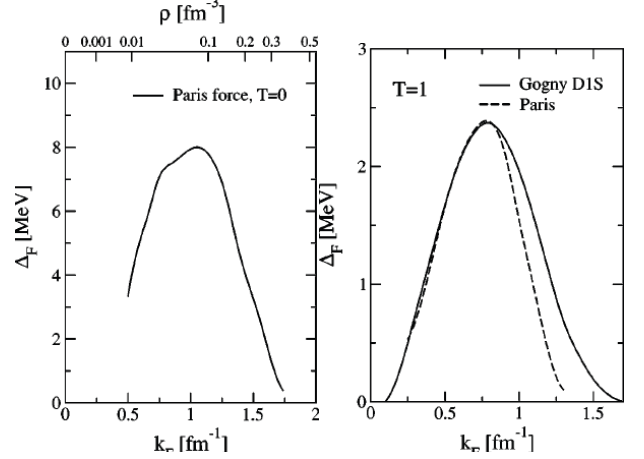


Fig. 5: Fermi momentum dependence of the pairing gaps, for the $T = 0$ spin-triplet and the $T = 1$ spin-singlet channels. The $T = 0$ results are calculated by using the Paris potential, while the $T = 1$ results are obtained by using either the Paris potential or the Gogny D1S effective force. The corresponding nuclear density is also given in the upper axis of the figure for the $T = 0$ case. The figures are taken from Ref. [24].

associated with the inner crust. The strong pairing at low density may also be relevant for finite nuclei, if one considers neutron-rich nuclei near the drip-line as, for example, ${}^6\text{He}$ and ${}^{11}\text{Li}$. This is because such nuclei are characterized by low-density distributions of neutrons around the nuclear surface (the so-called neutron skin and/or neutron halo). It is interesting to clarify to which extent the pair correlations in these exotic nuclei are different from those in stable nuclei, reflecting the strong density dependence of the pairing correlations. In fact, the di-neutron correlation in the two-neutron halo nuclei such as ${}^{11}\text{Li}$, in which a spatially correlated pair formed by the halo neutrons shows up, may be considered as a manifestation of the strong pairing correlations in low-density regime. A recent theoretical analysis using the HFB method [46] also predicts the presence of similar di-neutron correlations in medium-mass neutron-rich nuclei where more than two weakly-bound neutrons contribute to create the neutron skin in the outer part of the nuclear surface.

It has been argued that the BCS superconducting phase will change to a strong coupling regime, or Bose-Einstein condensate (BEC) phase made up with spatially compact, bound Fermion pairs if the pairing strength becomes strong enough to drive a phase transition. The schematic solutions of the BCS equations [3] suggest that the relevant parameter in this respect is the pairing strength times the level density. In ordinary nuclei, the level density is as a rule too small to have a phase transition. Moreover, it is impossible to design systems where these parameters can be varied. Instead, the BCS-BEC crossover phenomenon was recently observed in ultra-cold atomic gases in a trap, for which the interaction is controllable [47]. In the case of the nuclear pairing, the BCS-BEC crossover has been argued mostly for the neutron-proton $T = 0$ pairing in the tensor coupled spin-triplet 3SD_1 channel, for which the strong deuteron-like spatial correlations may be the

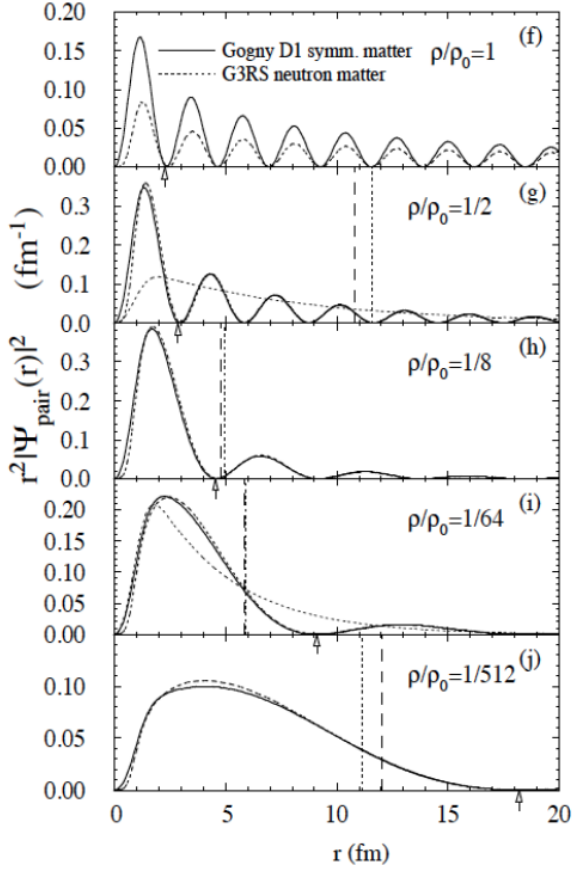


Fig. 6: The square of the wave function Ψ_{pair} of the neutron Cooper pair, as a function of the relative distance r between the pair partners, at the neutron density $\rho/\rho_0 = 1, 1/2, 1/8, 1/64, 1/512$. The solid curve is for the pair in symmetric nuclear matter calculated with the Gogny D1 force, while the dotted curve is for the pair in neutron matter calculated with the G3RS force (see also the main text). The vertical dotted line represents the r.m.s. radius of the Cooper pair in neutron matter, while the dashed line represents the same quantity in the case of nuclear matter. The arrow indicates the average inter-neutron distance d . The thin dotted line in (g) and (i) is the wave function of a fictitious bound state in the free space (this is calculated by increasing the pairing strength, so that a bound state appears, and tuning it so that the r.m.s. radius is the same of the real state whose wave function is displayed). The figure is taken from Ref. [48]

driving force, while at the same time uniform systems like matter in neutron stars can realize a situation where the level density is large. Concerning the neutron pairing in the $T = 1, S = 0$ channel, we may expect strong coupling regimes in the low density matter, such as unique di-neutron or di-proton correlations, whereas the transition to BEC phase is more questionable.

The pattern change of the spatial correlations of Cooper pairs in nuclear matter was discussed by M. Matsuo in Ref. [48]. The square of the wave function of the neutron Cooper pair is shown, as a function of the relative distance r between the two neutrons and at various densities, in Fig. 6. The solid curves show the results in symmetric nuclear matter obtained with the Gogny D1 force, while the dotted curves are the results in neutron matter obtained with G3RS force, which is a simple representation with three Gaussians of the bare force [49]. At normal nuclear density, the wave function has an oscillatory behaviour in the coordinate space and the coherence length ξ is large (the coherence length ξ is the measure of the size of the Cooper pair, defined in a similar way to the r.m.s. radius of wave function [3]). This is a typical BCS-type wave function in the weak-coupling pairing scheme. On the other hand, at lower density such as in the case in which $\rho/\rho_0 = 1/8$, the pairing correlations are strong enough to create a BEC-like wave function which has a short coherence length and is quite compact in coordinate space.

To move to finite, weakly-bound nuclei, we show in Fig. 7 the neutron pair wave function in ^{11}Li calculated by means of a three-body model that assumes the ^9Li core [42, 50]. The two-neutron wave function is calculated in the coordinate system where \vec{r}_1 and \vec{r}_2 are the distances of the two neutrons from the center of the core. This wave function is then written in terms of the relative distance \vec{r} between the two neutrons, and the distance \vec{R} between the core and the center of the two neutrons. The projected wave function on the total spin $S = 0$ state reads

$$\begin{aligned} & \Psi^{(S=0)}(\vec{r}_1, \vec{r}_2) \\ &= \sum_L f_L(r, R) [Y_L(\hat{r}) Y_L(\hat{R})]^{(00)} [\chi_{1/2} \chi_{1/2}]^{(00)}. \end{aligned} \quad (16)$$

The density dependent pairing interaction adopted in the three-body model calculations is strongly attractive near the surface, and rather weak near the center of nucleus, so that in terms of density dependence is quite similar to the realistic pairing interactions shown in Fig. 5. The pair wave function in general has two peaks in the two-dimensional plane (r, R) , as shown in the bottom-right corner of Fig. 7. There is a strong peak at large R and small r : this configuration is referred to as the "di-neutron" configuration. On the other hand, there is a smaller peak at large r and small R : this is called the "butterfly" configuration. The total spin (S) component of the di-neutron configuration is dominantly $S = 0$, while a large $S = 1$ component is found in the butterfly configuration.

The wave function associated with the di-neutron configuration is cut at different distances R from the center and shown as well in Fig. 7. Near the center of the core at $R = 0.5$ fm, the pair wave function has an oscillatory behavior similar to the nuclear matter result at the normal density $\rho/\rho_0 = 1$. When the value of R is increased and

the density becomes dilute, the oscillatory behavior gradually disappears and one finds a single peak at $R \approx 4$ fm, where the pairing correlations reach their maximum. This di-neutron wave function in ^{11}Li shows, therefore, a very similar behavior as the pair wave function in the nuclear matter that has been associated to the BCS-BEC crossover and shown in Fig. 6.

3. Competition between isoscalar and isovector pairing interaction

3.1. Pairing correlation energy for pf shell configurations

After having reviewed many general features of pairing in nuclei, we aim in this Section to point to some observation that can pin down, quantitatively, the interplay between isovector and isoscalar pairing. Certainly, pairing correlation energies are a quite direct observable: they represent the energy gain due to the pairing correlation.

We adopt in this case a separable form, namely the spin-singlet $T = 1$ pairing interaction reads in this case

$$V^{(T=1)}(\vec{r}_1, \vec{r}_2) = -G^{(T=1)} \sum_{i,j} P_{i,i}^{(1,0)\dagger}(\vec{r}_1, \vec{r}_2) P_{j,j}^{(1,0)}(\vec{r}_1, \vec{r}_2), \quad (17)$$

where the pair field operator is defined as

$$P_{i,j}^{(T,S)\dagger}(\vec{r}_1, \vec{r}_2) = \delta_{l_i, l_j} \sqrt{2l_i + 1} [a_i^\dagger a_j^\dagger]^{(T,S)} \psi_i(\vec{r}_1)^* \psi_j(\vec{r}_2)^*, \quad (18)$$

in terms of a single-particle wave function $\psi_i(\vec{r})$ having quantum numbers $i \equiv \{n_i, l_i, j_i\}$. Here, a_i^\dagger and a_i are the creation and annihilation operators for the single-particle configuration i , respectively. The pairing strength $G^{(T=1)}$ can be fitted to the empirical pairing gaps given by Eq. (4) [45, 3, 52], and turns out to be in this case

$$G^{(T=1)} = \frac{24}{A} \text{ MeV}. \quad (19)$$

Even though the value in Eq. (19) is a reasonable choice for calculations performed within a model space consisting of one major shell [45, 3, 52], the absolute value of the pairing strength should not be taken seriously since it depends on the model space adopted. It was pointed out in Ref. [53] that the separable form of pairing interaction is quite useful as much as the non-separable realistic Hamiltonians adopted, e.g., in shell model calculations.

The spin-triplet $T=0$ pairing can also be given by a similar separable form,

$$V^{(T=0)}(\vec{r}_1, \vec{r}_2) = -f G^{(T=1)} \sum_{i \geq i', j \geq j'} P_{i,i'}^{(0,1)\dagger}(\vec{r}_1, \vec{r}_2) P_{j,j'}^{(0,1)}(\vec{r}_1, \vec{r}_2), \quad (20)$$

where the scaling factor f is defined in close analogy as we have already done in Eqs. (7) and (8), and as we shall do below. This factor is varied between 1 and 2 in the following study of the pairing correlation energy [5].

We can now discuss the energy gain due to the pairing correlations, that is, the pairing correlation energy. Fig. 8 shows these energies for the p -orbit ($l = 1$) and the f -orbit

($l = 3$) configurations, as a function of the scaling factor f for the $T = 0$ pairing. The energies for both the $J^\pi = 0^+$ state with the isospin $T = 1$, and the $J^\pi = 1^+$ state with the isospin $T = 0$ are shown in the figure. In the case of the $T = 0$ pairing, we need to add to the Hamiltonian the spin-orbit splitting parametrized as

$$\Delta \varepsilon_{ls} = -V_{ls}(\vec{l} \cdot \vec{s}), \quad (21)$$

where the spin-orbit coupling strength V_{ls} is taken to be [45]

$$V_{ls} = \frac{24}{A^{2/3}} \text{ MeV}. \quad (22)$$

This spin-orbit potential reproduces well the empirical spin-orbit splitting $\Delta \varepsilon = 7.0$ MeV between the $1f_{7/2}$ and $1f_{5/2}$ states in ^{41}Ca [54].

We diagonalize the pairing Hamiltonian separately for the p - and f -orbit configurations in order to disentangle the roles of the pairing and of the spin-orbit interactions in a transparent way. It should be noticed that, for the $T = 0$ pairing, the pair configurations are constructed not only with two equal orbitals having ($l_i = l_{i'}, j_i = j_{i'}$) but also with the spin-orbit partner orbits *viz.* ($l_i = l_{i'}, j_i = j_{i'} \pm 1$), as is seen in the two-body $T = 0$ pairing matrix elements discussed in the Appendix [cf. Eq. (57)]. Thus, in the $l = 1$ case, the $(2p_{3/2})^2$ and $(2p_{1/2})^2$ configurations are available for the $T = 1, J^\pi = 0^+$ state, while also the $(2p_{3/2}2p_{1/2})$ configuration is available for the $T = 0, J^\pi = 1^+$ state. In a similar way, the $(1f_{7/2})^2$ and $(1f_{5/2})^2$ configurations participate to the $J^\pi = 0^+$ state in the $l = 3$ case, and also the $(1f_{7/2}1f_{5/2})$ configuration is involved in the $J^\pi = 1^+$ state.

As one can see in Fig. 8, the lowest energy state with $J^\pi = 0^+$ for the $l = 3$ case gains more binding energy than the $J^\pi = 1^+$ state if the factor f is smaller than 1.5. In the strong $T = 0$ pairing case, that is, $f \geq 1.6$, the $J^\pi = 1^+$ state obtains more binding energy than the lowest $J^\pi = 0^+$ state. These results are largely due to the quenching of the $T = 0$ pairing matrix element by the transformation coefficient from the jj to LS coupling schemes [5]. This quenching never happens for the $T=1$ pairing matrix element, since the mapping of the two-particle wave function between the two coupling schemes is simply implemented by a factor $\sqrt{j+1/2}$ in Eq. (55). In the $l = 1$ case, the competition between the $J^\pi = 0^+$ and the $J^\pi = 1^+$ states is also seen in Fig. 8. Because of the smaller spin-orbit splitting in this case, the couplings among the available configurations are rather strong, and the lowest $J^\pi = 1^+$ state gains more binding energy than the $J^\pi = 0^+$ state in the case of $f \geq 1.4$. These results are consistent with the observed spins of $N = Z$ odd-odd nuclei in the pf shell, where all the ground states have the spin-parity $J^\pi = 0^+$, except for $^{58}_{29}\text{Cu}$. The ground state of $^{58}_{29}\text{Cu}$ has $J^\pi = 1^+$, since the odd proton and odd neutron occupy mainly the $2p$ orbits, where the spin-orbit splitting is expected to be much smaller than that of $1f$ orbits.

The mass number dependence of the spin-orbit splitting is approximately determined by Eq. (22). Since the strength of the spin-orbit potential and the largest angular momentum in each major shell are proportional to $A^{-2/3}$ and $A^{1/3}$ [2], respectively, the spin-orbit splitting of the largest angular momentum states is roughly proportional

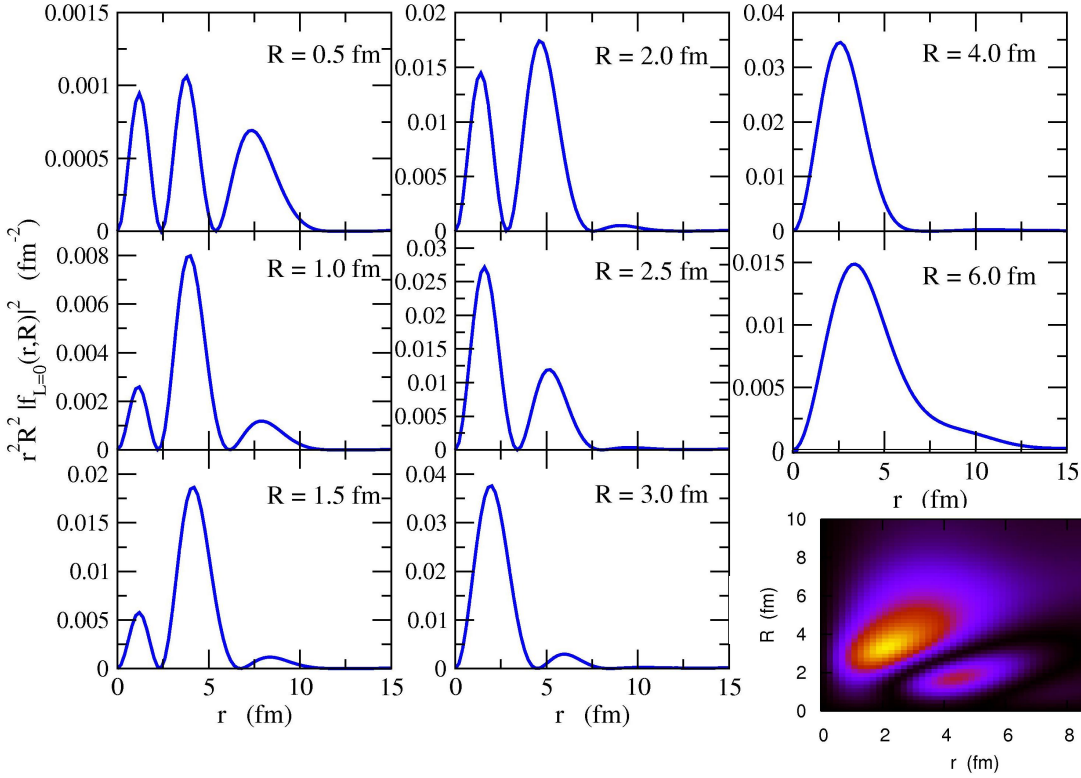


Fig. 7: The square of wave function $f_{(L=0)}(r, R)$ of the neutron pair as a function of the relative distance r between the neutrons. The bottom-right corner shows a 2D plot of the square of the wave function $f_{(L=0)}(r, R)$. The figure is taken from Ref. [51]

to $A^{-1/3}$. On the other hand, the $T = 0$ pairing matrix elements (57) for the separable interaction are proportional to the product of the pairing strength $G^{(T=0)}$ and the angular momentum of the valence orbit. This $T = 0$ pairing matrix element is thus expected to be proportional to $A^{-1} \times A^{1/3} = A^{-2/3}$. Thus, the spin-orbit splitting decreases more slowly than the pairing matrix element as a function of the mass number A . As a result, the spin-orbit splitting hinders more effectively the spin-triplet pairing correlations in medium-heavy nuclei with $N = Z > 30$ compared with lighter nuclei with $N = Z < 30$. We should also mention that, in reality, the spin-orbit splitting decreases even more slowly than predicted by the approximate $A^{-1/3}$ dependence: that is, it is found to be 6.2 MeV for the $l = 1$ states in ^{16}O , 5.5 MeV for the $l = 2$ states in ^{40}Ca , 7.0 MeV for the $l = 3$ states in ^{56}Ni , and 7.0 MeV for the $l = 4$ states in ^{100}Sn [2, 36].

As mentioned above, the shell model matrix elements are consistent with a factor f in Eq. (20) in the range of 1.6-1.7, for both sd shell and pf shell configurations [55, 56, 57]. In Ref. [52], the ratio 1.5 is adopted to analyze the spin-triplet pairing correlations in the $N = Z$ nuclei within shell model calculations. These adopted values of f , together with the results shown in Fig. 8, suggest that, in the odd-odd $N = Z$ nuclei, the configuration with $J^\pi = 1^+$ is favored in the ground state rather than the $J^\pi = 0^+$ one, especially when the $p_{3/2}$ orbit is the main configuration for the valence particles. However the onset of spin-triplet pair condensation is not guaranteed

by the simple inspection of the spin of the ground state, and may need a careful examination of many-body wave functions emerging from HFB or large-scale shell model calculations [58].

3.2. IAR and Gamow-Teller states in normal nuclei

3.2.1. RPA model and formalism

We recall here the main features of charge-exchange RPA and QRPA in the standard matrix formulation. The elementary excitations are either proton particle-neutron hole pairs of the type $a_{\alpha,\pi}^\dagger a_{\beta,\nu}$, or neutron particle-proton hole pairs of the type $a_{\alpha,\nu}^\dagger a_{\beta,\pi}$. Without pairing correlations, i.e., when the ground-state is HF, the index α (β) labels in what follows the unoccupied (occupied) states. Within the linear response theory, or RPA, the excited states $|n, \pm\rangle$ result from the action of the operators $\Gamma_{n,\pm}^\dagger$ on the correlated RPA ground state denoted by $|\tilde{0}\rangle$ for a nucleus with proton number Z . The RPA states have well-defined ΔT_z , and here the label \pm distinguishes the T_- and T_+ modes leading respectively to the $Z + 1$ and $Z - 1$ nuclei. The RPA operators can be expressed as follows:

$$\begin{aligned}\Gamma_{n,-}^\dagger &= \sum_{\alpha,\beta} X_{\alpha,\nu;\beta,\pi}^{(n)} a_{\alpha,\pi}^\dagger a_{\beta,\nu} - \sum_{\alpha,\beta} Y_{\alpha,\nu;\beta,\pi}^{(n)} a_{\beta,\pi}^\dagger a_{\alpha,\nu}, \\ \Gamma_{n,+}^\dagger &= \sum_{\alpha,\beta} X_{\alpha,\nu;\beta,\pi}^{(n)} a_{\alpha,\nu}^\dagger a_{\beta,\pi} - \sum_{\alpha,\beta} Y_{\alpha,\pi;\beta,\nu}^{(n)} a_{\beta,\nu}^\dagger a_{\alpha,\pi}.\end{aligned}\tag{23}$$

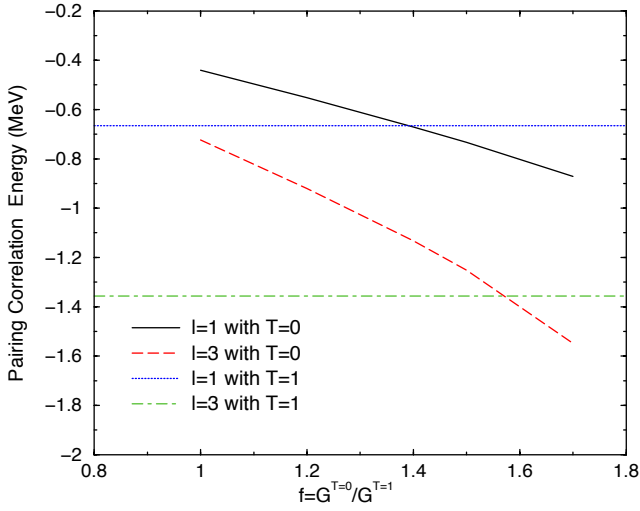


Fig. 8: The pairing correlation energies for the lowest ($J^\pi = 0^+, T = 1$) and ($J = 1^+, T = 0$) states in the case of the $l = 3$ and $l = 1$ configurations, as a function of the scaling factor f for the $T = 0$ pairing, defined in Eq. (20). The strength of the spin-singlet $T = 1$ pairing interaction is chosen to be $G^{(T=1)} = 24/A$ MeV with fixed mass number $A = 56$, while the strength for the spin-triplet $T = 0$ pairing, $G^{(T=0)}$, is varied as it is equal to the factor f multiplied by $G^{(T=1)}$. This figure is taken from Ref. [5].

With the additional assumption that the correlated RPA ground state is the vacuum for the RPA operators $\Gamma_{n,\pm}$ one can show that the $X^{(n)}, Y^{(n)}$ amplitudes define the eigenvectors of the following RPA secular matrix (where the indices α and β have been dropped for simplicity):

$$\begin{pmatrix} A_{\pi\nu,\pi'\nu'} & 0 & 0 & B_{\pi\nu,\nu'\pi'} \\ 0 & A_{\nu\pi,\nu'\pi'} & B_{\nu\pi,\pi'\nu'} & 0 \\ 0 & -B_{\pi\nu,\nu'\pi'} & -A_{\pi\nu,\pi'\nu'} & 0 \\ -B_{\nu\pi,\pi'\nu'} & 0 & 0 & -A_{\nu\pi,\nu'\pi'} \end{pmatrix} \times \begin{pmatrix} X_{\pi\nu}^{(n)} \\ X_{\nu\pi}^{(n)} \\ Y_{\pi\nu}^{(n)} \\ Y_{\nu\pi}^{(n)} \end{pmatrix} = E_n \begin{pmatrix} X_{\pi\nu}^{(n)} \\ X_{\nu\pi}^{(n)} \\ Y_{\pi\nu}^{(n)} \\ Y_{\nu\pi}^{(n)} \end{pmatrix}. \quad (24)$$

The corresponding eigenvalues E_n are the excitation energies of the RPA modes. The expressions of the A and B matrices are

$$\begin{aligned} A_{\pi\nu,\pi'\nu'} &\equiv A_{\alpha\pi,\beta\nu;\alpha'\pi',\beta'\nu'} \\ &= (\varepsilon_\alpha - \varepsilon_\beta) \delta_{\alpha\alpha'} \delta_{\beta\beta'} + \langle \alpha\beta' | V_{\text{ph}} | \beta\alpha' \rangle, \\ B_{\pi\nu,\nu'\pi'} &\equiv B_{\alpha\pi,\beta\nu;\alpha'\nu',\beta'\pi'} = \langle \alpha\alpha' | V_{\text{ph}} | \beta\beta' \rangle, \end{aligned} \quad (25)$$

and similarly for the other cases. In these formulas the single-particle energies ε and the matrix elements of the residual particle-hole (p-h) interaction V_{ph} appear. At variance with the case of normal RPA, the A matrix breaks into two blocks having different dimensions, and the matrix B is made up with two rectangular blocks. Under the spherical symmetry assumption the RPA excited states have good angular momentum and parity J^π and therefore, each J^π -mode corresponds to a separate diagonalization in the corresponding J^π p-h space. In this case,

all previous expressions can be cast in angular momentum coupled form: the final result is that the matrix equation (24) retains its structure and the matrix elements are coupled in this way: in $\langle \alpha\beta' | V_{\text{ph}} | \beta\alpha' \rangle$ the coupling is between $(\alpha \otimes \beta)_J$ and similarly $(\alpha' \otimes \beta')_J$.

In open-shell nuclei pairing correlations must be taken into account and, within the HFB framework the independent particles are replaced by quasi-particles so that RPA becomes QRPA. Quasi-particles are mixtures of particles and holes. If we use the symbol α^\dagger (α) for the quasi-particle creation (annihilation) operator, the QRPA modes are generated by

$$\Gamma_n^\dagger = \sum_{\alpha,\pi;\beta,\nu} X_{\alpha,\pi;\beta,\nu}^{(n)} \alpha_{\alpha,\pi}^\dagger \alpha_{\beta,\nu}^\dagger - Y_{\alpha,\pi;\beta,\nu}^{(n)} \alpha_{\beta,\nu} \alpha_{\alpha,\pi}. \quad (26)$$

Also this formula, and the following ones, can be recast in angular momentum coupled form. Similarly as in RPA, in QRPA also the states have well-defined ΔT_z . The QRPA matrix equation has the form

$$\begin{pmatrix} A_{\pi\nu,\pi'\nu'} & B_{\pi\nu,\pi'\nu'} \\ -B_{\pi\nu,\pi'\nu'} & -A_{\pi\nu,\pi'\nu'} \end{pmatrix} \begin{pmatrix} X_{\pi\nu}^{(n)} \\ Y_{\pi\nu}^{(n)} \end{pmatrix} = E_n \begin{pmatrix} X_{\pi\nu}^{(n)} \\ Y_{\pi\nu}^{(n)} \end{pmatrix}, \quad (27)$$

where once more the indices α and β have been dropped. The matrix elements appearing in the last formula include both the particle-hole and the particle-particle (p-p) residual interaction. QRPA can be built on top of HFB, or on top of the simpler HF-BCS approximation. The QRPA matrix elements display a quite similar form in the HF-BCS case and in the HFB case, provided one uses the canonical basis. They read

$$\begin{aligned} A_{\pi\nu,\pi'\nu'} &= (E_{\alpha,\alpha'} \delta_{\beta\beta'} + E_{\beta,\beta'} \delta_{\alpha\alpha'}) \\ &+ (u_\alpha v_\beta u_{\alpha'} v_{\beta'} + v_\alpha u_\beta v_{\alpha'} u_{\beta'}) \langle \alpha\beta' | V_{\text{ph}} | \beta\alpha' \rangle \\ &+ (u_\alpha u_\beta u_{\alpha'} u_{\beta'} + v_\alpha v_\beta v_{\alpha'} v_{\beta'}) \langle \alpha\beta | V_{\text{pp}} | \alpha'\beta' \rangle, \\ B_{\pi\nu,\pi'\nu'} &= (u_\alpha v_\beta v_{\alpha'} u_{\beta'} + v_\alpha u_\beta u_{\alpha'} v_{\beta'}) \langle \alpha\alpha' | V_{\text{ph}} | \beta\beta' \rangle \\ &- (u_\alpha u_\beta v_{\alpha'} v_{\beta'} + v_\alpha v_\beta u_{\alpha'} u_{\beta'}) \langle \alpha\beta | V_{\text{pp}} | \alpha'\beta' \rangle. \end{aligned} \quad (28)$$

Here u and v are the usual unoccupation and occupation factors, respectively, either of the BCS or of the canonical states. $E_{\alpha\alpha'}$ is either $E_\alpha \delta_{\alpha\alpha'}$ (being E_α the BCS quasi-particle energy), or the canonical basis matrix element of the HFB Hamiltonian.

Having the (Q)RPA amplitudes $X^{(n)}$ and $Y^{(n)}$ at one's disposal, it is possible to calculate the transition probability of the state $|\nu\rangle$ associated with a given operator \hat{O} . It is clear that a state characterized by many p-h or two quasi-particle configurations that do contribute coherently in the sum, possesses a large transition strength. The strength function is defined as

$$S(E) = \sum_\nu |\langle n | \mathcal{O}_\pm | \tilde{0} \rangle|^2 \delta(E - E_n), \quad (29)$$

and its moments are

$$m_k = \int dE E^k S(E) = \sum_\nu |\langle n | \mathcal{O}_\pm | \tilde{0} \rangle|^2 E_n^k. \quad (30)$$

Note that quite different ingredients are used even in self-consistent RPA or QRPA by different groups. In the

case of Skyrme calculations, the spin-isospin component of the residual interaction in the p-h channel is supplemented by a zero-range p-p force. In the case of RMF calculations, in the residual interaction the pion exchange is introduced; since this has no contribution for the ground-state which is treated at the Hartree level, the corresponding coupling constant must be fitted. In the case of RHF, the pion is introduced and fitted at the ground-state level: however, its role is modest in the residual interaction, and the position of the charge-exchange states turn out to be mainly determined by the exchange terms associated with the isoscalar σ and ω mesons [59]. Pairing is usually treated non-relativistically, both in RMF and RHF. This is important to be kept in mind, because even if our focus is on pairing effects, they cannot be completely decoupled from the underlying mean field.

3.2.2. Results

As we have mentioned already, we expect that the IAR is sensitive, in open-shell nuclei, to only or mainly $T = 1$ pairing. In the previous Section it is clearly shown that the p-n matrix elements enter in the QRPA residual interaction. It could be possible to just fit these matrix elements. Although, generally, one adopts pairing strengths of the order of what predicted by Eq. (19), the p-p and n-n empirical matrix elements have been often taken with different strengths: for instance, the values $G_n = 21/A$ and $G_p = 26/A$ have been adopted in Ref. [60]. However, the Coulomb (anti-)pairing effect should be taken into account and yet few groups have done it intensively [61]. This effect may reduce the pairing gaps by 100-200 keV [62] which means between about 5% and 20%. Therefore, it is legitimate to assume that the pairing force is isospin invariant, as all other components of any bare and/or effective nuclear forces are. In this case, one can say that ground-state 0^+ p-p and n-n matrix elements are equal to the p-n ones.

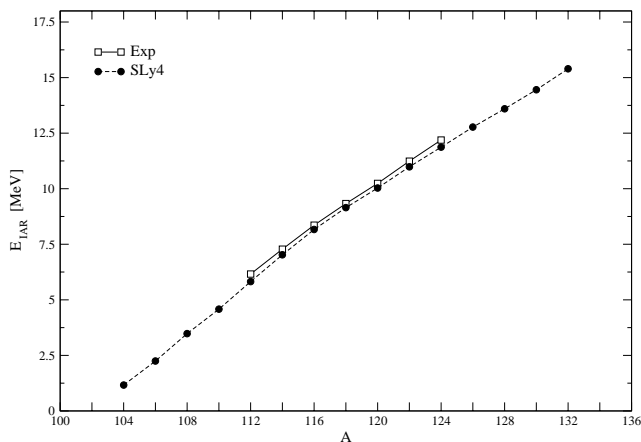


Fig. 9: Energies of the IAR in the Sn isotopes obtained by Skyrme-QRPA calculations are compared with experimental data from Ref. [65]. The figure is taken from Ref. [63].

At least, this is the attitude that has been adopted in

the context of both Skyrme [63] and RMF [64] calculations of the IAR, in which the $T = 1$ residual p-n matrix elements have been calculated consistently with the ground-state pairing force and the assumption of isospin invariance. The results for the IAR energies agrees very well with experiment (cf. Fig. 9), and it has been shown, moreover, that without p-n pairing in the residual interaction the IAR is fragmented in more than one peak and does not exhaust the whole $N - Z$ sum rule as it should.

The Gamow-Teller resonance is instead sensitive to the largely unknown p-n $T = 0$ pairing. Unfortunately, in standard nuclei this sensitivity is not strong enough to allow to pin down the strength of such pairing force. In Refs. [64] it has been found that the energy of the main GT peak in ^{118}Sn changes by at most 100 keV when the $T = 0$ pairing strength is changed by 50%. The inclusion of $T = 0$ pairing reduces the configuration splitting in the region of the main GTR, and has more influence generally speaking on the low-lying strength as it can be expected. In fact, it could be said that $T = 0$ pairing does play a role in the GT excitation spectra because of the partial occupations that are, in turn, induced by the $T = 1$ pairing in the ground state (this latter being, of course, more active around the Fermi surface).

As already discussed, the GT strength function is more sensitive to the spin-orbit splitting and p-h force. Nonetheless, it is interesting to notice that despite the rather different ansatz for such ingredients in the RMF and Skyrme frameworks, some of the conclusions reached in [27] are the same as in [64]. In particular, even in the Skyrme calculations of [27] the reduction of the configuration splitting due to $T = 0$ pairing has been observed. This has been specifically attributed to the attractive matrix elements of such force. For instance, in the case of ^{118}Sn , without $T = 0$ pairing the two QRPA states associated with (mainly) the $(\nu g_{9/2}, \pi g_{7/2})$ and $(\nu h_{11/2}, \pi h_{9/2})$ configurations are split considerably, the latter configuration being at higher energy than the former. However, due to the partial occupation of the $l = 5$ levels which is caused by the $T = 1$ pairing, they are quite sensitive to $T = 0$ pairing whose attractive matrix elements push the $(\nu h_{11/2}, \pi h_{9/2})$ downwards: thus, this configuration is finally more admixed in the wave function of the main resonance that it would happen without $T = 1$ pairing.

Although these effects are of some interest and could be detected experimentally in decay experiments, or other kinds of exclusive experiments, the need is clear for more direct evidences of $T = 1$ pairing. This will be the subject of the next subsections.

3.3. Gamow-Teller states and $T = 0$ pair in $N \approx Z$ nuclei

As is discussed above, pairing shows up in the QRPA equations through its contribution to the p-p matrix elements of the residual interaction. From the viewpoint of the QRPA model, for IAR states with $J^\pi = 0^+$, only $T = 1$ pairing provides a contribution, while for the GT states with $J^\pi = 1^+$, only $T = 0$ pairing contributes; for other spin-isospin transitions, such as spin-dipole and spin-quadrupole states, both $T = 0$ and $T = 1$ pairing provide contributions. Therefore, GT states are good can-

didates to study $T = 0$ pairing.

Due to selection rules, the GT transitions connect either single-particle states with $j_\nu = j_\pi$, or single-particle states with $j_\nu = j_\pi \pm 1$, while the IAR is only made up with the former type of transitions. Here, and in what follows, the notation $j_<$ ($j_>$) labels the spin-orbit partner with $j_< = l - 1/2$ ($j_> = l + 1/2$). Usually, the former type of transitions $\nu j_> \rightarrow \pi j_>$ or $\nu j_< \rightarrow \pi j_<$ is ≈ 3 -7 MeV lower (higher) in energy than the latter type of transitions $\nu j_> \rightarrow \pi j_<$ ($\nu j_< \rightarrow \pi j_>$) due to the spin-orbit splitting. These considerations would completely govern the unperturbed nuclear response. RPA correlations, however, play an important role and we can focus on the matrix elements appearing in the A matrix of Eq. (28), as they are more important than the matrix elements that fill up the matrix B , as a rule. In the particle-hole sector the coefficient including occupation factors reads $u_\alpha v_\beta u_{\alpha'} v_{\beta'}$, and is non-negligible mainly for configurations at relatively high excitation energy. On the other hand, in the particle-particle sector the relevant configurations are those made up with partially occupied states near the Fermi surface, that is, at relatively low excitation energy. Because of these reasons, the high-lying GT resonance is more sensitive to the p-h spin-isospin interaction, whose strength has been often related to the Landau-Migdal parameter g'_0 [32] as far as the central terms are concerned; tensor terms play also a role, in fact [33, 34]. For the low energy GT strength, the situation becomes much more complex [16]: in this case, the $T = 0$ pairing residual interaction plays a role and its strength can somehow be pinned down while, however, central and tensor terms of the p-h residual interaction are also important.

In order to study the GT transitions in $N \approx Z$ nuclei, we have applied the self-consistent Skyrme HFB+QRPA model. In the calculations, zero-range surface $T=0$ pairing was used and its form is the same as it has been shown in Eq. (12) with a scaling factor f , namely

$$V_{surface}^{T=0}(\vec{r}_1, \vec{r}_2) = \hat{P}_t f V_0 \left(1 - x \left(\frac{\rho}{\rho_0} \right)^\gamma \right) \delta(\vec{r}_1 - \vec{r}_2). \quad (31)$$

where \hat{P}_t is the projector on spin-triplet states.

3.3.1. Low energy GT state and $T = 0$ pairing in $N = Z$ nuclei

We have calculated the GT strength distribution in a series of $N = Z$ pf -shell nuclei ^{48}Cr , ^{56}Ni , and ^{64}Ge , and the results are shown in Fig. 10. We have performed these QRPA calculations by assuming different strengths for the $T = 0$ pairing or, in other words, the factor f is taken as 0.0, 0.5, 1.0, 1.5, and 1.7 in Eq. (31). The GT strength distribution of ^{64}Ge is shown in the panel (c), and it is evident that with the increasing of the $T = 0$ pairing strength, a small amount of GT strength is shifted to the low energy region while the energy of the low energy peak is shifted downwards albeit only slightly. In general only a small amount of GT strength is distributed in this low energy region, and this region is about 6 MeV lower than the high energy peak. This is the normal case of GT strength distributions, as is widely known in standard nuclei with considerable neutron excess. In the case of ^{56}Ni , the situation changes: when the $T = 0$ pairing is not included the

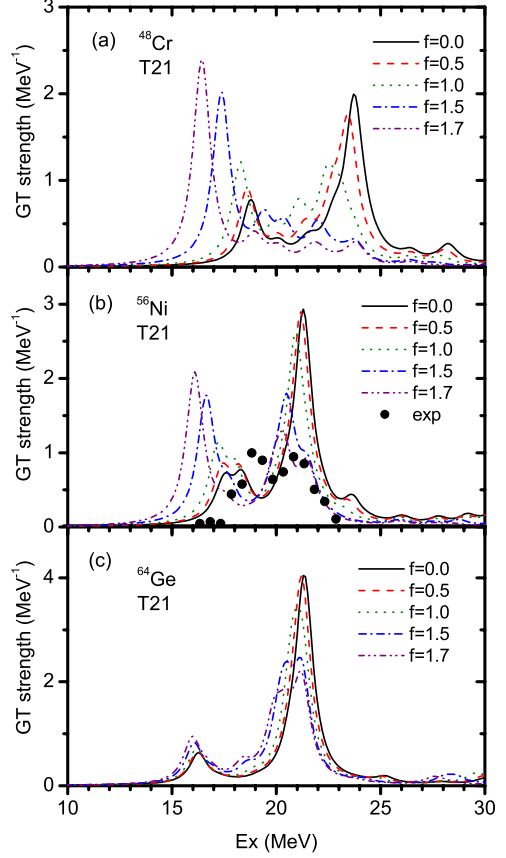


Fig. 10: GT strength distribution in $N = Z$ nuclei ^{48}Cr , ^{56}Ni , and ^{64}Ge calculated by HFB+QRPA with the Skyrme force T21 and with different strengths of $T = 0$ pairing. The excitation energies are calculated with respect to the mother nuclei. The experimental data are taken from [66]. The figure is taken from Ref. [67].

GT strength distribution is also like in the normal case, i.e. with a main peak in the high energy region and little amount of strength distributed at low energy (actually, if we do HF+RPA calculation, without pairing, there is only one peak). With the increase of the $T = 0$ pairing, the strength is shifted to the low energy region and meanwhile the low energy peak is shifted downward, in a more significant fashion than in the previous case. In particular, when $f = 1.5$, there are two peaks having similar amount of strength, and this is qualitatively consistent with the measured two peak structure [66]. However, as was commented by the authors of Ref. [68], the experimental results are not well reproduced by our present calculation; actually, there are other causes that may affect the peak energies in ^{56}Ni , such as the particle-vibration coupling (PVC) effect [69]. One might need to use well constrained Skyrme force together with theoretical model that go beyond QRPA, like QRPA plus PVC or second QRPA, if one wishes a good reproduction of experimental data [70]. For ^{48}Cr , the situation becomes quite extreme, that is, when the $T = 0$ pairing strength is strong enough (i.e., with $f = 1.5$ or 1.7), most GT strength is shifted to the low energy region and forms the main peak, whereas the original main peak in the high energy region calculated without

$T = 0$ pairing disappears. Thus, in this nucleus the $T = 0$ pairing might play a much more important role. Therefore, in some $N = Z$ nuclei, the $T = 0$ pairing may play an important role to shift a big amount of GT strength to the low energy region to form a strong GT state there. Interestingly, this happens for values of f that are very consistent with those extracted from shell model matrix elements and discussed in Ref. [25] as well as in our text above.

3.3.2. Low energy GT state and $T = 0$ pairing in $N = Z + 2$ nuclei

GT states in a series of $N = Z + 2$ pf -shell nuclei have been measured in Ref. [71], and it has been found that while in some nuclei the usual high-lying GTR is found, and no significant strength at low energy appears, in other cases the main GT peak is detected in the low energy region. In these cases, the main GT may exhaust more than 80% of the total strength, and it has been called Low energy Super Gamow-Teller (LeSGT) state.

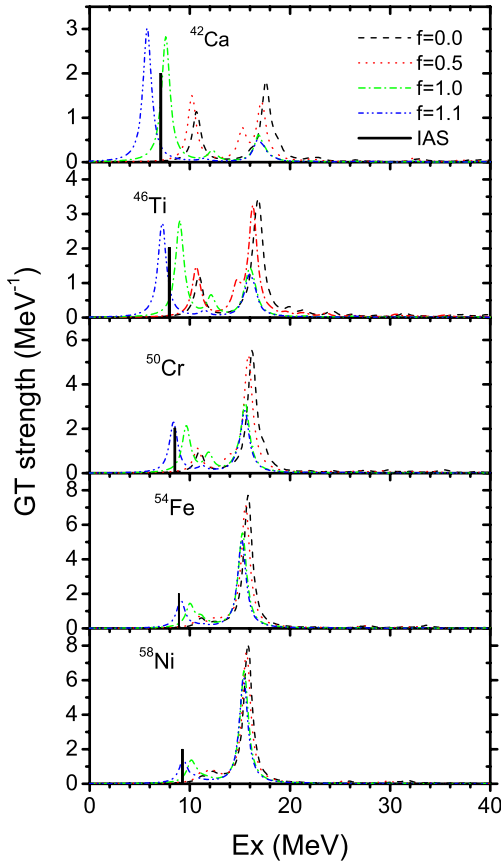


Fig. 11: GT strength distribution in $N = Z + 2$ nuclei with mass number between 42 and 58, calculated by means of HFB+QRPA with the Skyrme force SAMi and different strength of for the $T = 0$ pairing. The vertical black line corresponds to the IAR state. The excitation energies are calculated with respect to the mother nuclei. The figure is taken from Ref. [72].

The Skyrme HFB+QRPA results for the GT strength distribution in $N = Z + 2$ nuclei from $A = 42$ to 58 are

shown in Fig. 11. From this figure, one can see that in ^{42}Ca and ^{46}Ti the $T = 0$ pairing (assumed to have a strength similar to that of the corresponding $T = 1$ pairing) may shift a big amount of GT strength to the low energy region to form a strong GT state (LeSGT). Due to this reason, the high energy peak disappears. For ^{50}Cr , $T = 0$ pairing is also responsible for the shift of some amount of GT strength to the low energy region but its role is not as strong in the case of ^{42}Ca and ^{46}Ti . In ^{54}Fe and ^{58}Ni , the importance of $T = 0$ pairing further decreases.

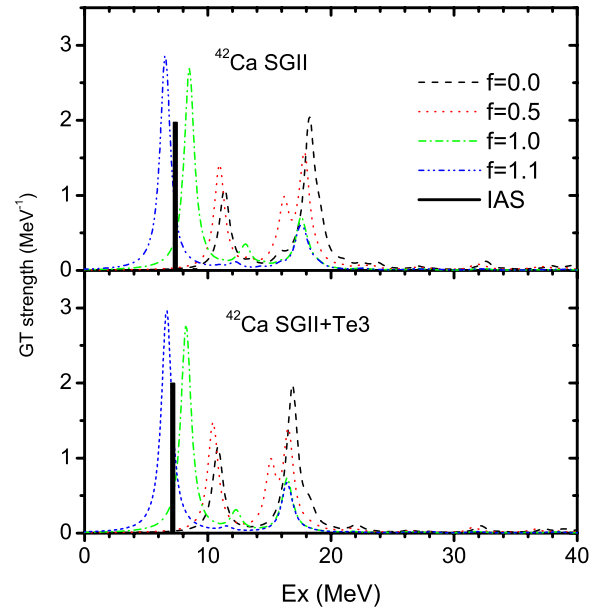


Fig. 12: GT strength distribution in ^{42}Ca calculated by means of HFB+QRPA with the Skyrme force SGII, with or without tensor force. The vertical black line corresponds to the IAR state. The excitation energies are calculated with respect to the mother nuclei. The figure is taken from Ref. [72].

The GT strength distributions in ^{42}Ca , calculated by means of HFB+QRPA with the Skyrme force SGII, with or without the tensor force, are shown in Fig. 12. In the upper (lower) panel, results without (with) the tensor force, are displayed. From this figure one can see that the tensor force plays an important role when the $T = 0$ pairing is not strong, i.e. when $f = 0.0$ and 0.5 . Instead, when f takes more realistic values like 1.0 or 1.1 , the strength distributions with and without tensor force are almost the same. This indicates that the tensor force effects are suppressed by the $T = 0$ pairing with proper strength, and this means that one can extract reliable information on $T = 0$ pairing from such nucleus.

This conclusion may change if another nucleus is chosen.

$$+V_{pn}(\vec{r}_p, \vec{r}_n) + \frac{(\vec{p}_p + \vec{p}_n)^2}{2A_C m}, \quad (32)$$

where m is the nucleon mass, A_C is the mass number of the core nucleus, and V_{pC} and V_{nC} are the mean field potentials for the valence proton and neutron, respectively, generated by the core nucleus. These are given as

$$V_{nC}(\vec{r}_n) = V^{(N)}(r_n), \quad V_{pC}(\vec{r}_p) = V^{(N)}(r_p) + V^{(C)}(r_p), \quad (33)$$

where $V^{(N)}$ and $V^{(C)}$ are the nuclear and the Coulomb parts, respectively. In Eq. (32), V_{pn} is the pairing interaction between the two valence nucleons. For simplicity, one can safely neglect the recoil kinetic energy of the core nucleus, that is, the last term in Eq. (32). The nuclear part of the core-valence particle interaction, Eq. (33), is taken to be

$$V^{(N)}(r) = v_0 f(r) + v_{ls} \frac{1}{r} \frac{df(r)}{dr} (\vec{l} \cdot \vec{s}), \quad (34)$$

where $f(r)$ is a Fermi function defined by $f(r) = 1/(1 + \exp[(r - R)/a])$. For the ^{18}F nucleus, as in Ref. [6], we set $v_0 = -49.21$ MeV and $v_{ls} = 21.6$ MeV·fm². For the other nuclei, we adjust v_0 so as to reproduce the neutron separation energies, while v_{ls} is kept constant for all the nuclei. For more details on the adopted parameters in the one-body potential, the reader can consult Ref. [6]. We use a contact interaction between the valence neutron and proton, V_{np} , that is the sum of $T = 0$ and $T = 1$ pairing forces with surface character as defined above in Eqs. (12) and (31). We write it here with inclusion of the appropriate projectors for the sake of clarity, namely

$$\begin{aligned} V_{np}(\vec{r}_1, \vec{r}_2) = & \hat{P}_s v_s \delta(\vec{r}_1 - \vec{r}_2) \left(1 - x_s \left(\frac{\rho(r)}{\rho_0}\right)^\gamma\right) \\ & + \hat{P}_t v_t \delta(\vec{r}_1 - \vec{r}_2) \left(1 - x_t \left(\frac{\rho(r)}{\rho_0}\right)^\gamma\right), \end{aligned} \quad (35)$$

where \hat{P}_s and \hat{P}_t are the projectors onto the spin-singlet and spin-triplet channels, respectively, defined in Eq. (9). Notice that the isovector spin-singlet pairing acts on even- J states $J^\pi = 0^+, 2^+, \dots (2j-1)^+$, while the isoscalar spin-triplet pairing acts on odd- J states $J^\pi = 1^+, 3^+, \dots (2j)^+$ for the configuration j^2 . In each channel in Eq. (35), the first term in brackets corresponds to the interaction in the vacuum while the second term takes into account the medium effects through the density dependence. Here, the core density is assumed to be a Fermi distribution of the same radius and diffuseness as in the core-valence particle interaction, Eq. (34). The strength parameters, v_s and v_t , are determined from the proton-neutron scattering length as [73]

$$v_s = \frac{2\pi^2 \hbar^2}{m} \frac{2a_{pn}^{(s)}}{\pi - 2a_{pn}^{(s)} k_{\text{cut}}}, \quad (36)$$

$$v_t = \frac{2\pi^2 \hbar^2}{m} \frac{2a_{pn}^{(t)}}{\pi - 2a_{pn}^{(t)} k_{\text{cut}}}, \quad (37)$$

where $a_{pn}^{(s)} = -23.749$ fm and $a_{pn}^{(t)} = 5.424$ fm [74] are the empirical p-n scattering lengths in the spin-singlet and

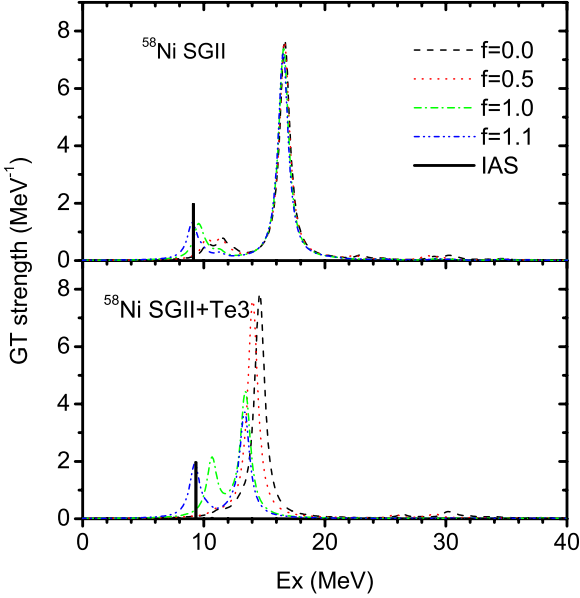


Fig. 13: Same as Fig. 13 in the case of ^{58}Ni . The figure is taken from Ref. [72].

From Fig. 13, we can see that the GT strength distributions with and without tensor force are quite different in ^{58}Ni even with strong $T = 0$ pairing strength. This means that in this case we do not have a unique signature of the effects of the $T = 0$ pairing from the low-energy GT strength.

Therefore, one can use the low energy GT states in ^{42}Ca and ^{46}Ti to extract reliable information on $T = 0$ pairing. Actually, the $T = 0$ pairing strength was suggested to be about 1.0 to 1.05 times the strength of corresponding $T=1$ pairing in Ref. [72]. Although this value is slightly smaller than what we have been discussed in Section 3.3.1, it has been extracted in a quite direct way. Qualitatively, it confirms that $T = 0$ pairing is stronger than $T = 1$ pairing.

3.4. Low-lying states in nuclei with one n-p pair outside the core

We focus in this Section on the energy spectra and spin-isospin excitations of odd-odd $N = Z$ sd - and pf - shell nuclei. To this end, we apply a three-body model with a density dependent contact interaction between the valence neutron and proton. The three-body model Hamiltonian for odd-odd $N = Z$ nuclei, assuming the core + $p + n$ structure [6], is given by

$$H = \frac{\vec{p}_p^2}{2m} + \frac{\vec{p}_n^2}{2m} + V_{pC}(\vec{r}_p) + V_{nC}(\vec{r}_n)$$

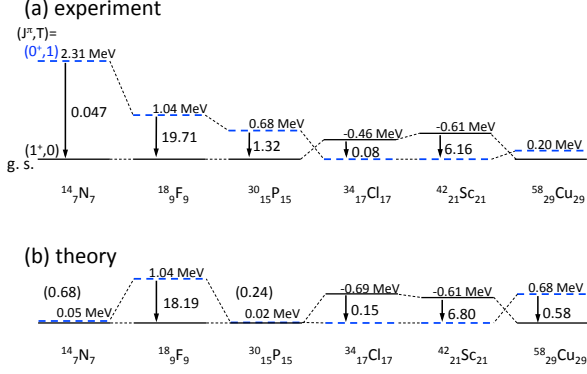


Fig. 14: (Color online) The energies of the first 0_1^+ and the first 1_1^+ states in $N = Z$ nuclei. The upper panel (a) shows experimental data and the lower panel (b) corresponds to calculated results. The values with the arrows show the transition probabilities for the magnetic dipole transitions, $B(M1)$ (the calculated values are shown in brackets for ^{14}N and ^{30}P). The experimental data are taken from Ref. [75].

spin-triplet channels, respectively. k_{cut} is the momentum cut-off that must be introduced when treating the delta function, and is related with the cutoff energy by $E_{\text{cut}} = \hbar^2 k_{\text{cut}}^2 / m$. In other words, the strengths v_s and v_t determined from the scattering lengths depend on the cut-off energy, E_{cut} . The three parameters x_s , x_t , and γ in the density dependent terms in Eq. (35) are determined so as to reproduce the energies of the ground state ($J^\pi = 1^+$), the first excited state ($J^\pi = 3^+$), and the second excited state ($J^\pi = 0^+$) in ^{18}F (see also Ref. [6]). The Hamiltonian (32) is diagonalized in the valence two-particle model space. The basis states for this diagonalization are given by a product of proton and neutron single particle states having single-particle energies $\epsilon^{(\tau)}$: these energies are obtained with the use of the single-particle potential $V_{\tau C}$ in Eq. (32) ($\tau = p$ or n). To this end, the single-particle continuum states are discretized in a large box. We include only those states satisfying $\epsilon_\alpha^{(p)} + \epsilon_\beta^{(n)} \leq E_{\text{cut}}$.

The calculated spectra for ^{14}N , ^{18}F , ^{30}P , ^{34}Cl , ^{42}Sc , and ^{58}Cu nuclei are shown in Fig. 14 together with the experimental data. The spin-parity for the ground state of the nuclei in Fig. 14 are $J^\pi = 1^+$ except for ^{34}Cl and ^{42}Sc . This feature is entirely due to the interplay between the isoscalar spin-triplet and the isovector spin-singlet pairing interactions in these $N = Z$ nuclei. In the present calculations, the ratio between the isoscalar and the isovector pairing interactions is $v_t/v_s = 1.9$ for the energy cutoff of the model space $E_{\text{cut}} = 20$ MeV. This ratio is somewhat larger than the value ≈ 1.6 extracted in Ref. [55] from the shell model matrix elements in p - and sd -shell nuclei and already discussed in the previous Sections. For a larger model space with $E_{\text{cut}} = 30$ MeV, the ratio becomes 1.6, but the agreement between the experimental data and the calculations somewhat worsens quantitatively even though the general features remain the same. It is remarkable that

the energy differences $\Delta E = E(0_1^+) - E(1_1^+)$ are well reproduced in ^{34}Cl and ^{42}Sc both qualitatively (there is an inversion between the 0^+ state and the 1^+ state that becomes the ground state) and quantitatively (if one looks at the absolute value of the energy difference). The model description is somewhat poor in ^{14}N and ^{30}P because the cores of these two nuclei are deformed: nevertheless, the ordering of the two lowest levels are correctly reproduced.

The probability of the total spin $S = 0$ and $S = 1$ components for the 0^+ and the 1^+ states, respectively, are listed in Table 1. The total spin $S = 0$ and $S = 1$ components in two particle configurations can be calculated with the formula

$$|(j_\pi j_\nu)J\rangle = \sum_{L,S} \left\{ \begin{matrix} l_\pi & l_\nu & L \\ s & s & S \\ j_\pi & j_\nu & J \end{matrix} \right\} \hat{L} \hat{S} \hat{j}_\pi \hat{j}_\nu |(l_\pi l_\nu)LS; J\rangle, \quad (38)$$

where $\hat{L}, \hat{S}, \hat{j}$ are $\hat{L} = \sqrt{2L+1}$, $\hat{S} = \sqrt{2S+1}$, $\hat{j} = \sqrt{2j+1}$, respectively. For a $j_\pi = j_\nu = j = l + 1/2$ configuration, the $S = 0$ and $S = 1$ components are given by the factors $(j+1/2)/2j$ and $(j-1/2)/2j$, respectively, for $J = 0$. For a $j_\pi = j_\nu = j = l - 1/2$ configuration, on the other hand, they are $(j+1/2)/(2j+2)$ and $(j+3/2)/(2j+2)$ for $S = 0$ and $S = 1$, respectively. Notice that the $s_{1/2}^2$ configuration has only $S = 0$ component if $J = 0$. Otherwise, all the two particle states have a large mixture of the $S = 0$ and $S = 1$ components. In general, the $S = 1$ and $S = 0$ components are thus largely mixed in the wave functions of both the ground and the excited states. An exception is ^{30}P . In this nucleus, the dominant configuration in the 0^+ state is $(2s_{1/2}^\pi \otimes 2s_{1/2}^\nu)$, which can couple only to the total spin $S = 0$. On the other hand, in the 1^+ state, the dominant configuration is $(2s_{1/2} \otimes 1d_{3/2})$ $T = 0$ which can couple only to the total spin $S = 1$ with the total angular momentum $L = 2$.

The reduced magnetic dipole transition probability is given by

$$B(M1 : J_i \rightarrow J_f) = \left(\frac{3}{4\pi} \right) \frac{1}{2J_i + 1} \left| \langle J_f || \sum_i (g_s(i) \vec{s}_i + g_l(i) \vec{l}_i) || J_i \rangle \right|^2, \quad (39)$$

where the double bar means a reduced matrix element in the spin space. We take the bare g factors $g_s(\pi) = 5.58$, $g_s(\nu) = -3.82$, $g_l(\pi) = 1$, and $g_l(\nu) = 0$ for the magnetic moments, and the magnetic dipole transitions are given in unit of the nuclear magneton $\mu_N = e\hbar/2mc$. The spin-quadrupole transition is defined instead by

$$B(IVSQ : J_i \rightarrow J_f) = \frac{1}{2J_i + 1} \left| \langle J_f || \sum_i r_i^2 [\vec{\sigma}(i) Y_2(i)]^{(\lambda=1)} \tau_z(i) || J_i \rangle \right|^2. \quad (40)$$

The calculated magnetic moments and magnetic dipole transitions are listed in Table 2 together with the spin quadrupole transitions. The calculated magnetic moment

Table 1: The energy difference between the 0_1^+ and 1_1^+ states, $\Delta E = E(0_1^+) - E(1_1^+)$, in $N = Z$ nuclei. The probabilities of the $S = 0$ component $P(S = 0)$ in the wave functions for the 0_1^+ state are shown in the fourth line. The fifth line shows the probability of the $S = 1$ component in the 1_1^+ state. The probabilities $P(j^\pi \otimes j^\nu)$ for the dominant valence shell proton-neutron configuration are also given for the 0_1^+ and 1_1^+ states in the seventh and eighth line, respectively. The experimental data are taken from Ref. [75].

		^{14}N	^{18}F	^{30}P	^{34}Cl	^{42}Sc	^{58}Cu
ΔE	exp.	2.31	1.04	0.68	-0.46	-0.61	0.20
(MeV)	cal.	0.05	1.04	0.02	-0.69	-0.61	0.68
$P(S = 0)$ (%)	0^+	34.8	82.2	94.8	40.7	70.5	65.4
$P(S = 1)$ (%)	1^+	78.3	90.1	95.8	64.3	65.7	92.1
j		$1p_{1/2}$	$1d_{5/2}$	$2s_{1/2}$	$1d_{3/2}$	$1f_{7/2}$	$2p_{3/2}$
$P(j^\pi \otimes j^\nu)$	0^+	97.2	85.2	89.7	98.6	94.2	81.2
(%)	1^+	96.4	52.1	1.1	98.4	82.7	10.0

in ^{14}N reproduces well the observed one, while the agreement is worse in ^{58}Cu . This is due to the fact that the core of ^{56}Ni might be largely broken and the $f_{7/2}$ hole configuration is mixed in the ground state of ^{58}Cu [76, 77]. The values for $B(M1)$ are also shown in Fig. 14. Very strong $B(M1)$ values are found both experimentally and theoretically in two of the $N = Z$ nuclei in Table 2, that is, in ^{18}F and ^{42}Sc .

The $B(M1)$ transition from 0^+ to 1^+ in ^{18}F is the largest one so far observed in the entire region of nuclear chart. We notice that our three-body calculations provide fine agreements not only for these strong transitions in ^{18}F and ^{42}Sc but also for the quenched transitions in the other $N = Z$ nuclei such as in ^{14}N and ^{34}Cl . The shell model calculation of Ref. [78] shows also a large enhancement for the $B(M1)$ transition in ^{18}F which is consistent with both the present study and the experiment.

In the case of ^{18}F , the 0^+ and 1^+ states are largely dominated by the $S = 0$ and $S = 1$ spin components, respectively, with orbital angular momentum $l = 2$ (see Table 1). Therefore, the two states can be considered as members of the $\text{SU}(4)$ multiplet in the spin-isospin space [79]. This is the main reason why the $B(M1)$ value is so large in this nucleus, since the spin-isospin operator $g_s^{IV} \vec{\sigma} \tau_z$ connects two states in the same $\text{SU}(4)$ multiplet, that is, the transition is allowed, and the isovector g -factor is the dominant term in Eq. (39) with $g_s^{IV} = (g_s(\nu) - g_s(\pi))/2 = -4.70$. The configurations in ^{42}Sc are also similar to those in ^{18}F in terms of $\text{SU}(4)$ multiplets, although they are dominated by $l = 3$ wave functions. For ^{14}N and ^{34}Cl , the $B(M1)$ transitions do not acquire any enhancement, since the $S = 0$ component in the 0^+ state is suppressed due to the $j = l - 1/2$ coupling: both the 0^+ and 1^+ states have very large $1p_{1/2}^2$ ($1d_{3/2}^2$) configurations in ^{14}N (^{34}Cl). These indications for the $\text{SU}(4)$ symmetry in ^{18}F and ^{42}Sc are consistent with the results obtained in Refs. [80, 81, 82].

In the nuclei ^{30}P and ^{58}Cu , the 1^+ state is dominated by $1d_{3/2}2s_{1/2}$ and $2p_{3/2}1f_{5/2}$ configurations, respectively, while the 0^+ state is governed by the $2s_{1/2}^2$ and $2p_{3/2}^2$ configurations, respectively. Therefore the isovector spin-quadrupole transitions are largely enhanced in the two nuclei even though the $B(M1)$ is much quenched. The validity of $\text{SU}(4)$ symmetry has been known already for

a quite long time in p -shell shell nuclei [83]. The two-body matrix element of Cohen-Kurath [84] for the spin-triplet $(J, T) = (1, 0)$ interaction is certainly stronger than that for the spin-singlet $(J, T) = (0, 1)$ pairing interaction. Then, the structure of the two-body wave function will be rather described by the LS coupling scheme than jj coupling scheme.

3.5. Gamow-Teller transitions in $N \approx Z$ nuclei by the three-body model

Some of us have applied the same three-body model as described in Subsection 3.4 to calculate the GT strength of $N = Z + 2$ nuclei. The Gamow-Teller (GT) transition strength reads

$$B(GT : 0^+ \rightarrow 1^+) = \frac{g_A^2}{4\pi} \left| \langle 1^+ | \sum_i t_-(i) \vec{\sigma}(i) | 0^+ \rangle \right|^2, \quad (41)$$

where g_A is the axial-vector coupling constant. The results are summarized in Table 3. One can again see a strong GT transition between the lowest 0^+ and 1^+ states in $A = 18$ and 42 systems, which exhausts a large portion of the GT sum rule value. This can also be interpreted as a manifestation of $\text{SU}(4)$ symmetry in the wave functions of these nuclei. We note also that the result obtained in Ref. [80] by an analysis of GT transitions also implies a good $\text{SU}(4)$ symmetry in the $A = 18$ system. On the other hand, for ^{58}Cu , the GT strength is largely fragmented and no state with a strong $B(GT)$ is seen near the ground state. The experimental data are consistent with the calculated results as can be seen in Table 3. The ratio of $B(GT)$ values from the ground states, between $A = 18, 42$ and 58 , is 1:0.69:0.05 if one takes the experimental values while the calculated ratio is 1:0.71:0.04 and is very close to the experimental one. This agreement suggests the validity of the three-body model wave functions in these nuclei.

Extensive shell model calculations have been performed in the full p -shell, sd -shell and pf -shell model spaces in the literature (cf. Refs. [84], [78] and [77], respectively). In these studies, the magnetic moments, M1 transitions and GT transitions were studied and the calculated results reproduce well the experimental observations. The

Table 2: The magnetic dipole transitions, and the isovector spin quadrupole transitions in the $N = Z$ nuclei are displayed. The experimental data for the $B(M1)$ values are taken from Ref. [75]. The symbol \downarrow (\uparrow) denotes a transition from the excited (ground) state to the ground (excited) state.

		^{14}N	^{18}F	^{30}P	^{34}Cl	^{42}Sc	^{58}Cu
J_{gs}^π		1^+	1^+	1^+	0^+	0^+	1^+
$B(M1) \downarrow (\mu_N^2)$	exp.	0.047	19.71	1.32	0.08	6.16	–
	cal.	0.682	18.19	0.24	0.15	6.81	0.580
$B(SQ) \uparrow (\text{fm}^4)$	cal.	33.17	0.85	43.04	74.52	19.61	71.55

Table 3: The Gamow-Teller transition probabilities from the ground states of ^{18}O to ^{18}F , ^{42}Ca to ^{42}Sc , and ^{58}Ni to ^{58}Cu , in units of $g_A^2/4\pi$. The experimental data are taken from Ref. [85] for ^{18}F , Ref. [86] for ^{42}Sc and Ref. [87] for ^{58}Cu , respectively.

$^{18}\text{O} \rightarrow ^{18}\text{F}$			
E_x (MeV)		$B(GT) (g_A^2/4\pi)$	
Th.	Exp.	Th.	Exp.
0.0	0.0	2.48	3.11 ± 0.03
4.79		0.028	
6.87		0.036	
$^{42}\text{Ca} \rightarrow ^{42}\text{Sc}$			
E_x (MeV)		$B(GT) (g_A^2/4\pi)$	
Th.	Exp.	Th.	Exp.
0.61	0.61	1.80	2.16 ± 0.15
	1.89		0.09 ± 0.02
3.71	3.69	0.346	0.15 ± 0.03
$^{58}\text{Ni} \rightarrow ^{58}\text{Cu}$			
E_x (MeV)		$B(GT) (g_A^2/4\pi)$	
Th.	Exp.	Th.	Exp.
0.0	0.0	0.097	0.155 ± 0.01
1.24	1.05	0.74	0.30 ± 0.04

validity of SU(4) symmetry in GT decays was also studied in terms of shell model calculations of p -shell nuclei in Ref. [88]. In contrast, our aim in this paper is not to compete with these complete shell model calculations, but to extract the role of the spin-singlet and the spin-triplet pairing interactions for the ground states and the excited states in the odd-odd $N = Z$ nuclei by the three-body model with one set of input data for the entire mass region, and to explore therefore the validity of SU(4) symmetry in the spin-isospin space simple terms. We should note that the present model is quite appropriate for ^{18}F and ^{42}Sc since ^{16}O and ^{40}Ca are double closed-shell nuclei and can be considered as good cores. On the other hand, the model space of the three-body model is not quite large enough for ^{30}P , ^{34}Cl and ^{58}Cu since excited states of the core might be coupled to the configurations of the present model space.

For ^{14}N , the two-hole three-body model might be more appropriate to adopt since ^{16}O is a better core than ^{12}C . With the density dependent, surface-type pairing [$x_s = x_t = +1$ in Eq. (35)], the energy difference between the 0^+ and 1^+ states becomes ≈ 2 MeV which is close to the experimental observation. However, the magnetic dipole transition becomes much larger than the observed one. It can be pointed out that the mixing of sd shell components will play an important role for the quenching of $B(M1)$ and $B(GT)$ values.

3.6. Pair transfer reactions

As it is intuitive and well known, two-particle transfer reactions are sensitive to the correlations between those particles, so that two-neutron transfer has been for long time used to pin down fingerprints of $T = 1$ pairing, and recently there is a strong interest to understand to which extent deuteron transfer can probe $T = 0$ pairing.

There are some basic problems, nonetheless, both at the conceptual and experimental level. Let us assume we can restrict to $L = 0$ states excited in transitions between even-even nuclei. Normal QRPA, or shell-model calculations, can provide the wave functions of such excited states n ; in particular, one can calculate the strength functions $S(E)$ associated either with the pair addition (ad) or pair removal (rm) operators. These strength functions read

$$\begin{aligned}
S_{\text{ad}} &= \sum_{n \in A+2} |\langle n | \hat{P}^\dagger | 0 \rangle|^2 \delta(E - E_n), \\
S_{\text{rm}} &= \sum_{n \in A-2} |\langle n | \hat{P} | 0 \rangle|^2 \delta(E - E_n),
\end{aligned} \tag{42}$$

where the sums run over the appropriate set of final states in the $A + 2$ or $A - 2$ nuclei, and $|0\rangle$ is the ground state of the even-even nucleus under study. The pair addition operators is

$$\hat{P}_{T=1, S=0}^{\dagger} (T=0, S=1) = \frac{1}{2} \sum_{\sigma, \sigma'} \sum_{\tau, \tau'} \int d^3r \hat{\psi}^{\dagger}(\vec{r}\sigma\tau) \langle \sigma\tau | \tau_z(\sigma_z) | \sigma'\tau' \rangle \hat{\psi}^{\dagger}(\vec{r}\sigma'\tau'), \quad (43)$$

where $\hat{\psi}^{\dagger}(\vec{r}\sigma\tau)$ is the nucleon field operator, and the time-conjugate state is defined by $\hat{\psi}^{\dagger}(\vec{r}\bar{\sigma}\bar{\tau}) \equiv (-2\sigma)(-2\tau)\hat{\psi}^{\dagger}(\vec{r}-\sigma-\tau)$. We have specifically singled out the S, T dependence. One can consider the neutron-neutron case [89] where only $J^{\pi} = 0^{+}, T = 1, S = 0$ is possible if $L = 0$, or the neutron-proton case [90] where either $J^{\pi} = 0^{+}, T = 1, S = 0$ or $J^{\pi} = 1^{+}, T = 0, S = 1$ are possible.

The strength functions (42) are known to be characterized by collective modes like pair vibrations and rotations [3]. A so-called giant pairing vibration (GPV) has been predicted long ago [91], and yet it has not been so far unambiguously identified despite many efforts that have been carried out since the 1970s until very recently (cf. [92] and references therein). One of the reasons that have been advocated is that GPVs are expected to lie at high energies, and the semi-classical condition of the optimal Q -value favors ground-state to ground-state transitions in the reactions with stable beams and targets (cf. [93] and references therein).

The interest has recently switched to the behaviour of such excitations far from stability, and to the issue whether this can bring information on pairing in neutron-rich nuclei. The strength functions (42) have been calculated for the Sn isotopes in Ref. [89]. It has been found that ground-state to ground-state transitions have large pair addition strength in $^{110-130}\text{Sn}$. In $^{132-140}\text{Sn}$, characteristic pair vibrational modes show up, whose strength is slightly smaller than that of the ground-state transitions but still large enough in terms of matrix elements associated with single-particle pair transfer. In these nuclei which are considerably neutron-rich, such vibrational modes have an extended radial tail, associated with contributions from continuum transitions. A signature of this fact resides in the participation of high angular momentum states with $l \geq 5$ in these modes. Pairing rotational modes show up instead in more neutron-rich nuclei. These states, and especially their collectivity, is very sensitive to the kind of pairing interaction that is employed like volume pairing as in (7) or surface pairing like in (12).

However, the pairing addition or pairing removal strength is not directly observable. The measurable quantity, namely the two-particle transfer cross section is not simply a factorized product of such matrix element times kinematical factors since the reaction process is quite involved. The full microscopic theory of the reaction process is explained in textbooks [94] and review papers [95]. Sophisticated calculations of absolute cross sections have been published starting from the 1960s (see e.g. [96] for a compact résumé and a survey of references), until the very recent state-of-the-art scheme of Ref. [97]. We do not wish here to give a full account of these calculations

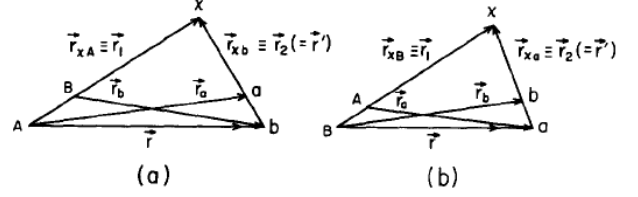


Fig. 15: Choice of coordinates appropriate for (a) stripping and (b) pick-up reactions. Figure taken from Ref. [99].

but simply convey the main points that are also connected to the similar difficulties that one may expect in the case of $T = 0$ pairing.

In a Distorted Wave Born Approximation (DWBA) picture, the reaction cross section associated with $A + a \rightarrow B + b$ will be proportional to the square of the transition amplitude. At variance with the inelastic case, the nucleons are in different partitions in the initial Aa and final Bb channels. One could define a *natural* coordinate system in each of these two initial and final channels, and in this way identify the two relative coordinates \vec{r}_a and \vec{r}_b in such channels (see e.g. Refs. [98, 99] for details and Fig. 15 for illustration). The projectile-target interaction can be defined either in the initial or final channel (where the words ejectile-residual could be more appropriate), and one refers to the two choices as prior or post representations, respectively. In case of a finite-range interaction V such features brings in many complications associated with non-localities. Neglecting them, that is, approximating $\vec{r}_a \approx \vec{r}_b \approx \vec{R}$ as in Eq. (17) of [95], the transition amplitude reads

$$T_{A+a \rightarrow B+b} \approx \int d^3R \chi_{Bb}^{\dagger}(\vec{r}_a, \vec{k}_f) F(\vec{R}) \chi_{Aa}(\vec{r}_b, \vec{k}_i), \quad (44)$$

where the χ are distorted wave functions that carry appropriate momentum labels, while F is the reaction form factor,

$$F(\vec{R}) \approx \langle \Psi_B \Psi_b | V | \Psi_A \Psi_a \rangle, \quad (45)$$

which is written in terms of intrinsic wave functions Ψ . We remind that the differential cross section is

$$\left(\frac{d\sigma}{d\Omega} \right) = |T_{A+a \rightarrow B+b}|^2. \quad (46)$$

What appears clearly, then, is that while the matrix elements that appear in Eq. (44) involve a full integration over space, in the form factor (45) the effective interaction V is active only in the range allowed by the reaction mechanism and acts a kind of filter that makes the connection between pairing correlations and reaction cross sections quite indirect.

In such a complicated situation, the comparison of the latest theoretical calculations of [97] with the experimental data from Ref. [100] have nonetheless provided strong evidence that our current understanding of $T = 1$ pairing is confirmed by the analysis of the results of (p,t) transfer reactions on the stable Sn isotopes. On the other hand, reaction cross section calculations have not been performed for neutron-rich and weakly bound isotopes e.g. beyond

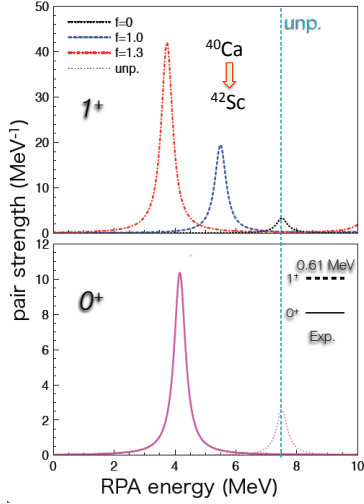


Fig. 16: (Color online) $L = 0$ neutron-proton pair addition strength (42) in the case of the transitions $^{40}\text{Ca} \rightarrow ^{42}\text{Sc}$. In the case of $J^\pi = 1^+$ states the operator $\hat{P}_{T=0, S=1}$ is active, whereas in the case of $J^\pi = 0^+$ states the strength is associated with $\hat{P}_{T=1, S=0}$. The sharp peaks associated with the strength function (42) are smeared by means of Lorentzian functions with a width of 0.1 MeV. In the $(J, T) = (1, 0)$ channel the spin-triplet pairing strength is changed by scaling factors $f = 0.0, 1.0$, and 1.3 [cf. Eq. (31)] while the spin-singlet pairing is fixed. The unperturbed pair transfer strength is also shown by a dotted line. In the lower panel, the experimental level scheme is inserted. This figure is based on the results of Ref. [90].

^{130}Sn . At present, such very neutron-rich nuclei are not yet available in such intensities that allow two-particle transfer reactions experiments but the topic is certainly of interest for the future.

It is quite obvious also to analyze whether neutron-proton transfer reactions can play a similar role as discussed so far, to pin down better evidences for $T = 0$ pairing. The issue has been recently discussed in Ref. [68]. One clear physics case would be to perform a reaction like $(^3\text{He}, p)$ on an even-even $N = Z$ nucleus. $N = Z$ nuclei are stable only up to ^{40}Ca . As the pairing collectivity is expected to be more pronounced for heavier systems, experimental programs for $(^3\text{He}, p)$ or $(^4\text{He}, d)$ reactions with unstable beams in inverse kinematics are strongly desired and called for. In such nuclei the $T = 0$ pairing correlations are expected to be enhanced as already discussed. Moreover, in that case one starts from a $T = 0, J^\pi = 0^+$ state and can probe the isospin invariance of $T = 1$ pairing by looking at the $T = 1, J^\pi = 0^+$ states in the odd-odd system and investigate $T = 0$ pairing by looking at the $T = 0, J^\pi = 1^+$ states.

A full theory like the one developed for equal-particle transfer reactions, that is, capable to predict absolute values of the cross section as we have just discussed, need still to be developed. This is one of the important priorities in the nuclear reaction domain. Meanwhile, if experimentally available, relative cross sections $\sigma(T = 0, J = 1^+)/\sigma(T = 1, J = 0^+)$ can provide first valuable information. It has to be noted that in such cross sections, strong interaction matrix elements that are exactly the analogous of the electromagnetic ones discussed in Sec. 3.4, play the important role.

The proton-neutron $L = 0$ pair transfer strength in the $N = Z$ nuclei ^{40}Ca and ^{56}Ni has been studied by K. Yoshida in Ref. [90] by using the proton-neutron RPA described in Sec. 3.2.1 with a Skyrme EDF. The pair addition strength of $^{40}\text{Ca} \rightarrow ^{42}\text{Sc}$ associated with both the $J^\pi = 1^+$ and $J^\pi = 0^+$ states is shown in Fig. 16. It was found that the collectivity of the lowest $J^\pi = 1^+$ in the neighboring odd-odd nucleus ^{42}Sc is stronger than that of the lowest $J^\pi = 0^+$ state when the IS spin-triplet pairing is taken to be equal or stronger than the IV spin-singlet pairing.

One sees that the excitation energy and the strength of the $J^\pi = 1^+$ states are strongly affected by the $T = 0$ pairing interaction. In the case of $f = 0$, without the $T = 0$ pairing interaction, the lowest 1^+ state in ^{42}Sc located at $\omega = 7.5$ MeV is a single-particle excitation $\pi f_{7/2} \nu f_{7/2}$. As the pairing interaction is switched on, and the strength is increased, the 1^+ state is shifted downwards in energy with the enhancement of the transition strength. With increasing pairing strength to $f = 1.0$ or 1.3 the lowest 1^+ state is constructed by many particle-particle excitations involving $f_{5/2}$ and $p_{3/2}$ orbitals located above the Fermi levels as well as the $\pi f_{7/2} \nu f_{7/2}$ excitation. It is particularly worth noting that the hole-hole excitations from the sd -shell have an appreciable contribution to generate this $T = 0$ proton-neutron pair-addition vibrational mode, indicating ^{40}Ca core-breaking. The strong collectivity is associated by a coherent phase of these configurations of pp and hh excitations.

4. Summary and Future perspectives

The superfluidity in nuclei was firstly pointed out in a milestone paper by A. Bohr, B.R. Mottelson and D. Pines in 1958. This historical paper has raised a strong impact on the study of nuclear superfluidity both from experimental and theoretical viewpoints. These studies have established solid evidences of superfluidity in nuclei such as the odd-even staggering in the mass systematics, the large energy gaps in the spectra of even-even nuclei, the quenching of the moment of inertia associated with rotational spectra of rare-earth deformed nuclei, and the enhancement of fission of actinide nuclei. Theoretically, the HF plus BCS and HFB theories have been developed and successfully applied to calculate the effect of pairing interactions on these phenomena.

It has also been pointed out that the pairing correlations will be much stronger in the lower density regime than at normal density. Nuclear matter calculations show the onset of the BCS-BEC crossover phenomenon in the low density regime, i.e., the spatial correlation of the Cooper pair is changing from a BCS-type behavior with a large coherence length at normal density to a BEC-type behavior with a compact coherence length. It was also pointed out that the weakly bound nuclei with halo or skin nature may show the strong di-nucleon correlations which give rise to a similar behaviour as in the BCS-BEC crossover when one studies the nucleon pairs as a function of the distance between the core and the center of the two nucleons.

So far, most of the studies of the pairing correlations have been concentrated on the isovector $T = 1$ spin-singlet pairing interaction. On the other hand, the isoscalar $T = 0$

spin-triplet pairing correlations could be much stronger than the $T = 1$ pairing ones. The importance of $T = 0$ spin-triplet pairing was already pointed out in the 1970s. There have been many discussions on possible signatures of the spin-triplet pairing correlations, such as the Wigner energy term in the mass formula, the enhancement of neutron-proton pair transfer cross sections, the inversion of $J = 0^+$ and $J = 1^+$ states, and the large enhancement of GT strength in the low-energy region of $N = Z$ and $N = Z + 2$ nuclei. However, so far no convincing evidence has been found about the spin-triplet superfluidity in nuclei. This may be due to the large spin-orbit splittings in the nuclear mean field and the large neutron excess $N > Z$ in stable nuclei with $A > 40$, which prevent the formation of spin-triplet Cooper pairs in nuclei.

In our paper, we have pointed out that the inversions of $J = 0^+$ and $J = 1^+$ states in the odd-odd $N = Z$ nuclei can be considered as a manifestation of strong spin-triplet pairing correlations. These nuclei also display strong magnetic dipole transitions that can be explained by the introduction of $T = 0$ pairing. Another kind of spin-dependent transition are the Gamow-Teller excitations from even-even $N = Z + 2$ to the neighbouring odd-odd ones. We have shown that the strong concentration of GT strength at low energy, close to the ground state of daughter nuclei, can be understood by QRPA calculations only with a strong $T = 0$ spin-triplet pairing interaction. In all these cases, the strength of the $T = 0$ pairing is larger, or slightly larger, than the strength of the $T = 1$ pairing, in agreement with similar conclusions extracted from the analysis of the shell model matrix elements.

A direct evidence of the strong neutron-proton pairing correlations could appear in the enhancement of the pair transfer cross sections. Several theoretical studies show clear signs of the strong pairing correlations in the two-nucleon pairing strength. However, the reaction process of two-nucleon transfer reactions is very involved. While some calculations have been performed in the case of two-neutron transfer, and are consistent with the assumptions on $T = 1$ pairing coming from other pieces of evidence, the study of proton-neutron transfer reactions is still in its infancy and more effort should be put on this topic.

The spin-triplet superfluidity is a fascinating subject for theoretical and experimental study. In the future, it would be highly interesting to build a realistic model able to predict the two-particle transfer cross sections theoretically, and point to possible spin-triplet pairing modes in the pair transfer reactions such as (^3He , p) or (p, ^3He).

A large amplitude collective motion such as fission is also very sensitive to whether the nucleus is a viscous fluid or a superfluid. Qualitatively, it is definitely true that superfluidity enhances the fission probability significantly. The fission induced by low-energy excitations which occur in neutron capture reactions are now feasible to be studied by microscopic theories like time-dependent HFB. These theoretical studies can provide observables such as the internal energies of fission fragments which can be compared with experimental data. We expect that this may also be instrumental for our understanding of pairing in nuclei.

Acknowledgement

We would like to thank Y. Fujita, K. Hagino, T. Sasano, Y. Tanimura, T. Uesaka, A. Vitturi for fruitful discussions and comments.

A. Two-body matrix elements of δ -type and separable pairing interactions

A.1. δ -type pairing interaction

We adopt the helicity representation to derive simple formulas involving only Clebsh-Gordan coefficients [45, 50]. In the helicity representation, the single-particle wave function reads

$$\psi_{nljm} = R_{nlj}(r) \left(\frac{2j+1}{16\pi^2} \right)^{1/2} \sum_{h=\pm 1/2} \alpha(ljh) D_{mh}^j(\hat{r}) \chi_h, \quad (47)$$

where $R_{nlj}(r)$, D_{mh}^j and χ_h are the radial wave function and D -function in the helicity function, respectively, and

$$\alpha(ljh) = (-)^{(h+1/2)(j-l-1/2)}. \quad (48)$$

The two particle wave function can be written for the contact interaction $\delta(\vec{r}_1 - \vec{r}_2)$ with $\hat{r}_1 = \hat{r}_2$ as

$$\begin{aligned} \Psi(\alpha\beta)_{JM} &= \frac{1}{\sqrt{1 + \delta_{\alpha,\beta}}} \sum_{h_\alpha, h_\beta} \langle j_\alpha h_\alpha j_\beta h_\beta | JH \rangle D_{MH}^J(\hat{r}) \\ &\times R_\alpha(r) R_\beta(r) \frac{\hat{j}_\alpha \hat{j}_\beta}{16\pi^2} \alpha(l_\alpha j_\alpha h_\alpha) \alpha(l_\beta j_\beta h_\beta) \chi_{h_\alpha} \chi_{h_\beta}, \end{aligned} \quad (49)$$

where $\alpha \equiv (n_\alpha l_\alpha j_\alpha)$ and $\hat{j} = (2j+1)^{1/2}$. To derive Eq. (49) we use the addition and the orthogonality relations of the D -functions (see Ref. [45] for details). For the total spin $S = 0$ state, the helicity H is restricted to be $H = 0$ only. By using the helicity representation of the two-particle state, the two-body matrix element for the contact pairing for the isovector spin-singlet channel $V^{(T=1, S=0)}(\mathbf{r}) = G^{(T=1)} f(\rho) \delta(\mathbf{r})$ is calculated to be

$$\begin{aligned} &\langle \Psi(\alpha'\beta')_{JM} | V^{(T=1, S=0)} | \Psi(\alpha\beta)_{JM} \rangle = \\ &\frac{1}{\sqrt{1 + \delta_{\alpha,\beta}}} \frac{1}{\sqrt{1 + \delta_{\alpha',\beta'}}} \langle j_\alpha 1/2 j_\beta -1/2 | J0 \rangle \\ &\langle j'_\alpha 1/2 j'_\beta -1/2 | J0 \rangle \frac{\hat{j}_\alpha \hat{j}_\beta \hat{j}'_\alpha \hat{j}'_\beta}{16\pi(2J+1)} \\ &\times (-)^{(j_\alpha - l_\alpha - 1/2 + j'_\alpha - l'_\alpha - 1/2)} [1 + (-)^{(l_\alpha + l_\beta + l'_\alpha + l'_\beta)}] \\ &\times I^{(T=1)}, \end{aligned}$$

where I is the radial integral

$$I^{(T=1)} = \int dr r^2 R_\alpha R_{\alpha'} R_\beta R_{\beta'} G^{(T=1)} f(\rho). \quad (50)$$

Here the $T = 1$ pairing strength is $G^{(T=1)}$ and the density dependent form factor is written as $f(\rho)$. For the anti-symmetrized state $\tilde{\Psi}$, the two body matrix elements will be

$$\begin{aligned} &\langle \tilde{\Psi}(\alpha'\beta')_{JM}^T | V^{(T=1, S=0)} | \tilde{\Psi}(\alpha\beta)_{JM}^T \rangle = \\ &\langle \Psi(\alpha'\beta')_{JM}^T | V^{(T=1, S=0)} \{ | \Psi(\alpha\beta)_{JM}^T \rangle \} \end{aligned}$$

$$\begin{aligned}
& -(-)^{j_\alpha+j_\beta-J-T-1} |\Psi(\beta\alpha)_{JM}^T \rangle = \\
& \frac{1}{\sqrt{1+\delta_{\alpha,\beta}}} \frac{1}{\sqrt{1+\delta_{\alpha',\beta'}}} \times \langle j_\alpha 1/2 j_\beta - 1/2 | J0 \rangle > \\
& \langle j'_\alpha 1/2 j'_\beta - 1/2 | J0 \rangle > \frac{\hat{j}_\alpha \hat{j}_\beta}{8\pi} \frac{\hat{j}'_\alpha \hat{j}'_\beta}{(2J+1)} \\
& \times (-)^{(j_\alpha-l_\alpha-1/2+j'_\alpha-l'_\alpha-1/2)} [1 + (-)^{(l_\alpha+l_\beta+J)}] \\
& \times I^{(T=1)}. \tag{51}
\end{aligned}$$

For the spin-triplet case, we have to calculate not only the $H = 0$ state, but also $H = \pm 1$ states. The $H = 0$ state give the same 2-body matrix element as the spin-singlet case (51) except for the J selection term which will be $[1 - (-)^{(l_\alpha+l_\beta+J)}]$ in the $S = 1$ case. We will present how to calculate the matrix element for the $H = -1$ state in the following. The matrix element for $H = 1$ is essentially the same as that of $H = -1$ state. The two-particle state for the total helicity $H = -1$ reads

$$\begin{aligned}
\Psi(\alpha\beta)_{JM} &= \frac{1}{\sqrt{1+\delta_{\alpha,\beta}}} \langle j_\alpha - 1/2 j_\beta - 1/2 | J-1 \rangle > \\
&\times D_{M-1}^J(\hat{r}) R_\alpha(r) R_\beta(r) \frac{\hat{j}_\alpha \hat{j}_\beta}{16\pi^2} \chi_{-1/2} \chi_{-1/2}, \tag{52}
\end{aligned}$$

where $\alpha(ljh)$ in Eq. (49) becomes always $+1$ for $h = -1/2$ state. The two-body matrix element of the $S = 1, H = -1$ state for the isoscalar spin-triplet interaction $V^{(T=0,S=1)} = G^{(T=0)} f(\rho) \delta(\mathbf{r})$ will be

$$\begin{aligned}
& \langle \Psi(\alpha'\beta)_{JH=-1}' | V^{(T=0,S=1)} | \Psi(\alpha\beta)_{JH=-1} \rangle = \\
& \frac{1}{\sqrt{1+\delta_{\alpha,\beta}}} \frac{1}{\sqrt{1+\delta_{\alpha',\beta'}}} \langle j_\alpha - 1/2 j_\beta - 1/2 | J-1 \rangle > \\
& \langle j'_\alpha - 1/2 j'_\beta - 1/2 | J-1 \rangle > \frac{\hat{j}_\alpha \hat{j}_\beta \hat{j}'_\alpha \hat{j}'_\beta}{16\pi(2J+1)} \\
& \times (-)^{j_\alpha+j'_\alpha+j_\beta+j'_\beta} \times I^{(T=0)},
\end{aligned}$$

where the radial integral $I^{(T=0)}$ has the pairing strength $G^{(T=0)}$ instead of $G^{(T=1)}$ in Eq. (50). This formula (53) can be rewritten further by using a recursion formula

$$\begin{aligned}
& \langle j_\alpha - 1/2 j_\beta - 1/2 | J-1 \rangle = \langle j_\alpha 1/2 j_\beta - 1/2 | J0 \rangle > \\
& \times \frac{(-)^{j_\alpha+j_\beta-J} (j_\alpha + 1/2) + (j_\beta + 1/2)}{[J(J+1)]^{1/2}}. \tag{53}
\end{aligned}$$

Then, the two-body matrix element becomes

$$\begin{aligned}
& \langle \Psi(\alpha'\beta)_{JH=-1}' | V^{(T=0,S=1)} | \Psi(\alpha\beta)_{JH=-1} \rangle = \\
& \frac{1}{\sqrt{1+\delta_{\alpha,\beta}}} \frac{1}{\sqrt{1+\delta_{\alpha',\beta'}}} \langle j_\alpha 1/2 j_\beta - 1/2 | J0 \rangle > \\
& \times \langle j'_\alpha 1/2 j'_\beta - 1/2 | J0 \rangle > \\
& \times \frac{(-)^{j_\alpha+j_\beta-J} (j_\alpha + 1/2) + (j_\beta + 1/2)}{[J(J+1)]^{1/2}} \\
& \times \frac{(-)^{j'_\alpha+j'_\beta-J} (j'_\alpha + 1/2) + (j'_\beta + 1/2)}{[J(J+1)]^{1/2}} \frac{\hat{j}_\alpha \hat{j}_\beta \hat{j}'_\alpha \hat{j}'_\beta}{16\pi(2J+1)} \\
& \times (-)^{j_\alpha+j'_\alpha+j_\beta+j'_\beta} \times I^{(T=0)}.
\end{aligned}$$

We have to sum up three terms $H = 0, H = \pm 1$ for the matrix element of the $S = 1$ state. We remind that $H =$

$+1$ state gives the same matrix element as that of $H = -1$ state. Eventually, for the anti-symmetrized $S = 1$ state, the two-body matrix element is given by

$$\begin{aligned}
& \langle \tilde{\Psi}(\alpha'\beta')_{JM}^{(T=0)} | V^{(T=0,S=1)} | \tilde{\Psi}(\alpha\beta)_{JM}^{(T=0)} \rangle = \\
& \frac{1}{\sqrt{1+\delta_{\alpha,\beta}}} \frac{1}{\sqrt{1+\delta_{\alpha',\beta'}}} \times \langle j_\alpha 1/2 j_\beta - 1/2 | J0 \rangle > \\
& \langle j'_\alpha 1/2 j'_\beta - 1/2 | J0 \rangle > \frac{\hat{j}_\alpha \hat{j}_\beta}{8\pi} \frac{\hat{j}'_\alpha \hat{j}'_\beta}{(2J+1)} \\
& \times (-)^{j_\alpha-l_\alpha-1/2+j'_\alpha-l'_\alpha-1/2} [(1 + (-)^{l_\alpha+l_\beta+J+1}) \\
& + 2(-)^{j_\beta+j'_\beta+l_\alpha+l'_\alpha+1} \frac{(-)^{j_\alpha+j_\beta-J} (j_\alpha + 1/2) + (j_\beta + 1/2)}{[J(J+1)]^{1/2}} \\
& \times \frac{(-)^{j'_\alpha+j'_\beta-J} (j'_\alpha + 1/2) + (j'_\beta + 1/2)}{[J(J+1)]^{1/2}}] \\
& \times I^{(T=0)}. \tag{54}
\end{aligned}$$

A.2. Separable pairing interaction

Let us discuss next the separable pairing interaction, i.e., the spin-singlet $T = 1$ pairing interaction (17) and the spin-triplet $T = 0$ pairing interaction (20). The two-body matrix element for the $T = 1$ pairing is evaluated to be

$$\begin{aligned}
& \langle (j_i j_i) T = 1, J = 0 | V^{(T=1)} | (j_j j_j) T = 1, J = 0 \rangle \\
& = -\sqrt{(j_i + 1/2)(j_j + 1/2)} G^{(T=1)} I_{ij}^2, \tag{55}
\end{aligned}$$

where I_{ij} is the overlap integral given by

$$I_{ij} = \int \psi_i(\mathbf{r})^* \psi_j(\mathbf{r}) d\mathbf{r}. \tag{56}$$

For the $T = 0$ pairing, the two-body matrix element involves the coefficient for the transformation from the jj coupling scheme to the LS coupling scheme, and is given by

$$\begin{aligned}
& \langle (j_1 j_2) T = 0, J = 1 | V^{(T=0)} | (j'_1 j'_2) T = 0, J = 1 \rangle = \\
& - \left\langle \left[\left(l_1 \frac{1}{2} \right)^{j_1} \left(l_2 \frac{1}{2} \right)^{j_2} \right]^{J=1} \left[\left(l_1 l_2 \right)^{L=0} \left(\frac{1}{2} \frac{1}{2} \right)^{S=1} \right]^{J=1} \right\rangle \\
& \times \left\langle \left[\left(l'_1 \frac{1}{2} \right)^{j'_1} \left(l'_2 \frac{1}{2} \right)^{j'_2} \right]^{J=1} \left[\left(l'_1 l'_2 \right)^{L=0} \left(\frac{1}{2} \frac{1}{2} \right)^{S=1} \right]^{J=1} \right\rangle \\
& \times \frac{\sqrt{2l_1+1} \sqrt{2l'_1+1}}{\sqrt{1+\delta_{j_1,j_2}} \sqrt{1+\delta_{j'_1,j'_2}}} f G^{(T=1)} (I_{j_1 j'_1} I_{j_2 j'_2} + I_{j_1 j'_2} I_{j_2 j'_1}),
\end{aligned}$$

Table 4: The transformation coefficient R between the jj coupling and the LS coupling for the pair wave functions, $R = \langle [(l_1 \frac{1}{2})^j (l_2 \frac{1}{2})^{j'}]^{J=1} | [(ll)^{L=0} (\frac{1}{2} \frac{1}{2})^{S=1}]^{J=1} \rangle$. Ω is defined as $\Omega \equiv 3(2l+1)^2$.

j	j'	R	$l = 1$	$l = 3$
$l + 1/2$	$l + 1/2$	$\sqrt{\frac{(2l+2)(2l+3)}{2\Omega}}$	$\frac{1}{3} \sqrt{\frac{10}{3}}$	$\frac{2\sqrt{3}}{7}$
$l + 1/2$	$l - 1/2$	$-\sqrt{\frac{4l(l+1)}{\Omega}}$	$-\frac{2}{3} \sqrt{\frac{2}{3}}$	$-\frac{4}{7}$
$l - 1/2$	$l - 1/2$	$-\sqrt{\frac{2l(2l-1)}{2\Omega}}$	$-\frac{1}{3} \sqrt{\frac{1}{3}}$	$-\frac{\sqrt{5}}{7}$
$l - 1/2$	$l + 1/2$	$\sqrt{\frac{4l(l+1)}{\Omega}}$	$\frac{2}{3} \sqrt{\frac{2}{3}}$	$\frac{4}{7}$

where $\langle [(l_1 \frac{1}{2})^{j_1} (l_2 \frac{1}{2})^{j_2}]^{J=1} | [(l_1 l_2)^{L=0} (\frac{1}{2} \frac{1}{2})^{S=1}]^{J=1} \rangle$ is the transformation coefficient, and the overlap integral I_{ij} involves both the proton and neutron wave functions. The transformation coefficient can be evaluated with the 9j symbol [cf. Eq. (38)] and the explicit form is summarized in Table 4. The square of the transformation coefficient is 1/6 and 1/3 for $j_1 = j_2$ and $j_1 = j_2 \pm 1$ configurations, respectively, in the limit of large angular momentum $l \rightarrow \infty$. These values suggest a large quenching of the spin-triplet pairing correlations, and that spin-orbit partners contribute largely to the spin-triplet pairing matrix elements. On the other hand, in the small l limit, $l \rightarrow 0$, the coefficient is unity for $j = j' = l + 1/2$, and the coefficients are zero for the other three configurations. This suggests that the spin-triplet pairing is as large as the spin-singlet pairing for the pair configuration in the $s_{1/2}$ orbit, and that it is still substantially large for the configuration in the $p_{3/2}$ orbit.

References

- [1] A. Bohr, B.R. Mottelson, D. Pines, Phys. Rev. **110**, 936 (1958).
- [2] A. Bohr, B.R. Mottelson, *Nuclear Structure. Volume I* (W.A. Benjamin, Inc., New York, 1969).
- [3] D.M. Brink, R.A. Broglia, *Nuclear Superfluidity. Pairing in Finite Systems* (Cambridge Monographs on Particle Physics, Nuclear Physics and Cosmology, vol. 24, 2005).
- [4] G.F. Bertsch, in *50 years of nuclear BCS* (edited by R.A. Broglia and V. Zelevinsky, World Scientific, 2012).
- [5] H. Sagawa, Y. Tanimura and K. Hagino, Phys. Rev. **C87**, 034310 (2013).
- [6] Y. Tanimura, K. Hagino and H. Sagawa, Phys. Rev. **C86**, 044331 (2012).
- [7] D. Vautherin, Phys. Rev. **C7**, 296 (1973).
- [8] P. Ring and P. Schuck, *The Nuclear Many-Body Problem* (Springer-Verlag, Berlin-Heidelberg, 1980).
- [9] J. Dobaczewski, H. Flocard, and J. Treiner, Nucl. Phys. **A422**, 103 (1984).
- [10] M. Bender, P.-H. Heenen and P.-G. Reinhard, Rev. Mod. Phys. **75**, 121 (2003).
- [11] M. V. Stoitsov, J. Dobaczewski, W. Nazarewicz and P. Borycki, Int. J. Mass Spectr. **251**, 243 (2006).
- [12] T. Duguet, P. Bonche, P.-H. Heenen, and J. Meyer, Phys. Rev. **C65**, 014311 (2001).
- [13] J. Margueron, H. Sagawa and K. Hagino, Phys. Rev. **C76**, 064316 (2007); Phys. Rev. **C77**, 054309 (2008).
- [14] D.J. Rowe, *Nuclear Collective Motion* (Methuen, London, 1970).
- [15] J. Terasaki, J. Engel, M. Bender, J. Dobaczewski, W. Nazarewicz, and M. Stoitsov, Phys. Rev. **C71**, 034310 (2005).
- [16] J. Engel *et al.*, Phys. Rev. **C60**, 014302 (2000).
- [17] M. Matsuo, Nucl. Phys. **A696**, 371 (2001).
- [18] E. Khan *et al.*, Phys. Rev. **C66**, 024309 (2002).
- [19] N. Paar *et al.*, Phys. Rev. **C67**, 034312 (2003).
- [20] A.L. Goodman, Nucl. Phys. **A186**, 475 (1972).
- [21] A.L. Goodman, Phys. Rev. **C60**, 014311 (1999).
- [22] A. Poves, G. Martinez-Pinedo, Phys. Lett. **B430**, 203 (1988).
- [23] E. Garrido, P. Sarriguren, E. Moya de Guerra, and P. Schuck, Phys. Rev. **C60**, 064312 (1999).
- [24] E. Garrido, P. Sarriguren, E. Moya de Guerra, U. Lombardo, P. Schuck, and H.J. Schulze, Phys. Rev. **C63**, 037304 (2001).
- [25] G.F. Bertsch and Y. Luo, Phys. Rev. **C81**, 064320 (2010).
- [26] A. Gezerlis, G.F. Bertsch, and Y.L. Luo, Phys. Rev. Lett. **106**, 252502 (2011).
- [27] S. Fracasso and G. Colò, Phys. Rev. **C76**, 044307 (2007).
- [28] I.N. Borzov, and S. Goriely, Phys. Rev. **C62**, 035501 (2000).
- [29] K. Yoshida, Prog. Theor. Exp. Phys. **113D02** (2013).
- [30] J. Suhonen, O. Civitarese, Phys. Rep. **300**, 123 (1998).
- [31] N. Van Giai, and H. Sagawa, Phys. Lett. **B106**, 379 (1981).
- [32] M. Bender, J. Dobaczewski, J. Engel, W. Nazarewicz, Phys. Rev. **C65**, 054322 (2002).
- [33] C.L. Bai, H. Sagawa, H.Q. Zhang, X.Z. Zhang, G. Colò, F.R. Xu, Phys. Lett. **B675**, 28 (2009).
- [34] C.L. Bai, H.Q. Zhang, X.Z. Zhang, F.R. Xu, H. Sagawa, and G. Colò, Phys. Rev. **C79**, 041301(R) (2009).
- [35] F. Minato and C.L. Bai, Phys. Rev. Lett. **110**, 122501 (2013).
- [36] X. Roca-Maza, G. Colò and H. Sagawa, Phys. Rev. **C86**, 031306(R) (2012).
- [37] W. Satuła, J. Dobaczewski, and W. Nazarewicz, Phys. Rev. Lett. **81**, 3599 (1998).
- [38] T. Duguet, P. Bonche, P.-H. Heenen, and J. Meyer, Phys. Rev. **C65**, 014310 (2001).
- [39] A. Goodman, Adv. Nucl. Phys. **11**, 263 (1979).

- [40] L. Grodzins, Phys. Lett. **2**, 88 (1962); S. Raman, C. Nestor, and P. Tikkanen, At. Data Nucl. Data Tables **78**, 1 (2001).
- [41] J. Terasaki, J. Engel, and G.F. Bertsch, Phys. Rev. C **78**, 044311 (2008).
- [42] G.F. Bertsch and H. Esbensen, Ann. Phys. **209**, (1991) 327.
- [43] S.V. Tolokonnikov, S. Kamedzhiev, D. Voitenkov, S. Krewald, and E.E. Saperstein, Phys. Rev. C **84**, 064324 (2011).
- [44] B.G. Carlsson, J. Toivanen, and A. Pastore, Phys. Rev. C **86**, 014307 (2012).
- [45] A. Bohr and B.R. Mottelson, *Nuclear Structure. Volume II* (W.A. Benjamin Inc., New York, 1972).
- [46] N. Pillet, N. Sandulescu, P. Schuck, and J.-F. Berger, Phys. Rev. C **81**, 034307 (2010).
- [47] M. Greiner *et al.*, Nature **426**, 537 (2004).
- [48] M. Matsuo, Phys. Rev. C **73**, 044309 (2006).
- [49] R. Tamagaki, Prog. Theo. Phys. **39**, 91 (1968).
- [50] H. Esbensen and G.F. Bertsch, Nucl. Phys. A **542**, 319 (1992).
- [51] K. Hagino, H. Sagawa, J. Carbonell, and P. Schuck, Phys. Rev. Lett. **99**, 022506 (2007).
- [52] A. Poves and G. Martinez-Pinedo, Phys. Lett. B **430**, 203 (1998).
- [53] E. Moya de Guerra, A.A. Raduta, L. Zamick and P. Sarriguren, Nucl. Phys. A **727**, 3 (2003).
- [54] Y. Uozumi *et al.*, Phys. Rev. C **51**, 263 (1994).
- [55] G.F. Bertsch and Y. Luo, Phys. Rev. C **81**, 064320 (2010).
- [56] B.A. Brown and W.A. Richter, Phys. Rev. C **74**, 034315 (2006).
- [57] M. Honma, T. Otsuka, B.A. Brown and T. Mizusaki, Phys. Rev. C **69**, 034335 (2004); Eur. Phys. J. A **25** Suppl. 1, 499 (2005).
- [58] A. Gezelis, G.F. Bertsch and Y.L. Luo, Phys. Rev. Lett. **106**, 252502 (2011).
- [59] H.Z. Liang, N.V. Giai and J. Meng, Phys. Rev. Lett. **101**, 22502 (2005).
- [60] S.G. Nilsson and I. Ragnarsson, *Shapes and Shells in Nuclear Structure* (Cambridge University Press, Cambridge, 1995).
- [61] M. Anguiano, J.L. Egido, L.M. Robledo, Nucl. Phys. A **683**, 627 (2001).
- [62] S. Hilaire, J.-F. Berger, M. Girod, W. Satuła, and P. Schuck, Phys. Lett. B **531**, 61 (2002).
- [63] S. Fracasso and G. Colò, Phys. Rev. C **62**, 064310 (2005).
- [64] D. Vretenar, N. Paar, T. Nikšić, and P. Ring, Phys. Rev. Lett. **91**, 262502 (2003); N. Paar, T. Nikšić, D. Vretenar, and P. Ring, Phys. Rev. C **69**, 054303 (2004).
- [65] K. Pham *et al.*, Phys. Rev. C **51**, 526 (1995).
- [66] M. Sasano *et al.*, Phys. Rev. Lett. **107**, 202501 (2011).
- [67] C.L. Bai, H. Sagawa, M. Sasano, T. Uesaka, K. Hagino, H.Q. Zhang, X.Z. Zhang, and F.R. Xu, Phys. Lett. B **719**, 116 (2013).
- [68] S. Frauendorf and A.O. Machiavelli, Prog. Part. Nucl. Phys. **78**, 24 (2014).
- [69] Y.F. Niu, G. Colò, M. Brenna, P.F. Bortignon, and J. Meng, Phys. Rev. C **85**, 034314 (2012).
- [70] E. Litvinova, B. A. Brown, D.-L. Fang, T. Marketin, and R. G. T. Zegers, Phys. Lett. B **730**, 307 (2014).
- [71] Y. Fujita *et al.*, Phys. Rev. Lett. **112**, 112502 (2014).
- [72] C. L. Bai, H. Sagawa, G. Colò, Y. Fujita, H.Q. Zhang, X.Z. Zhang, and F.R. Xu, Phys. Rev. C **90**, 054335 (2014).
- [73] H. Esbensen, G.F. Bertsch, and K. Hencken, Phys. Rev. C **56**, 3054 (1997).
- [74] L. Koester and W. Nistler, Z. Phys. A **272**, 189 (1975).
- [75] Chart of Nuclides, National Nuclear Data Center (<http://www.nndc.bnl.gov/>).
- [76] A.E. Lisetskiy *et al.*, Phys. Rev. C **68**, 034316 (2003).
- [77] M. Honma, T. Otsuka, B.A. Brown, and T. Mizusaki, Phys. Rev. C **69**, 034335 (2004).
- [78] B.A. Brown and B.H. Wildenthal, Phys. Rev. C **28**, 2397 (1983); M.C. Etchegoyen, A. Etchegoyen, B.H. Wildenthal, B.A. Brown and J. Keinonen, Phys. Rev. C **38**, 1382 (1988).
- [79] E.P. Wigner, Phys. Rev. **51**, 106 (1937); F. Hund, Z. Physik **105**, 202 (1937).
- [80] P. Halse and B.R. Barrett, Ann. Phys. (N. Y.) **192**, 204 (1989).
- [81] P. Vogel and W.E. Ormand, Phys. Rev. C **47**, 623 (1993).
- [82] P. Van Isacker, D.D. Warner, and D. S. Brenner, Phys. Rev. Lett. **74**, 4607 (1995).
- [83] M. Harvey, Adv. Nucl. Phys. **1**, 67 (1968); J.C. Parikh, *Group Symmetries in Nuclear Structure* (Plenum Press, New York, 1978).
- [84] S. Cohen and D. Kurath, Nucl. Phys. **73**, 1 (1965).
- [85] D.R. Tilley, H.R. Weller, C.M. Cheves and R.M. Chasteler, Nucl. Phys. A **595**, 1 (1995).

- [86] T. Kurtukian Nieto *et al.*, Phys. Rev. **C80**, 035502 (2009); Y. Fujita, private communication.
- [87] Y. Fujita *et al.*, Eur. Phys. J. **A13**, 411 (2002); Y. Fujita, private communication.
- [88] D. J. Millener, Eur. Phys. J. **A25**, s01, 97 (2005).
- [89] H. Shimoyama and M. Matsuo, Phys. Rev. **C88**, 054308 (2013).
- [90] K. Yoshida, Phys. Rev. **C90**, 031303(R) (2014).
- [91] D.R. Bès and R.A. Broglia, Nucl. Phys. **A80**, 289 (1966).
- [92] B. Mouginot *et al.*, Phys. Rev. **C83**, 037302 (2011).
- [93] L. Fortunato, W. von Oertzen, H.M. Sofia and A. Vitturi, Eur. Phys. J. **A14**, 37 (2002).
- [94] N.K. Glendenning, *Direct Nuclear Reactions* (Academic Press, New York, 1983).
- [95] W. Von Oertzen and A. Vitturi, Rep. Prog. Phys. **64**, 1247 (2001).
- [96] I.J. Thompson and B.A. Brown, in *50 Years of Nuclear BCS* (World Scientific, Singapore, 2013).
- [97] G. Potel, F. Barranco, F. Marini, A. Idini, E. Viguzzi, R.A. Broglia, Phys. Rev. Lett. **107**, 092501 (2011).
- [98] N. Austern, R.M. Drisco, E.C. Halbert, and G.R. Satchler, Phys. Rev. **133**, B3 (1964).
- [99] T. Tamura, Phys. Rep. **14**, 59 (1974).
- [100] P. Guazzoni *et al.*, Phys. Rev. **C60**, 054603 (1999); Phys. Rev. **C69**, 024619 (2004); Phys. Rev. **C74**, 054605 (2006); Phys. Rev. **C78**, 064608 (2008); Phys. Rev. **C83**, 044614 (2011).